Microstructure, Mechanical Properties and Texture Investigation of As-cast and Extruded AZ91 Mg Alloys

A THESIS

Submitted in partial fulfillment of the
requirements for the award of the degree
of
Master of Technology

by

Namrata Sarania

DEPARTMENT OF METALLURGICAL ENGINEERING AND MATERIALS SCIENCE

INDIAN INSTITUTE OF TECHNOLOGY INDORE

MAY 2023

INDIAN INSTITUTE OF TECHNOLOGY INDORE

CANDIDATE'S DECLARATION

I hereby certify that the work which is being presented in the thesis entitled "**Microstructure, Mechanical Properties and Texture Investigation of As-cast and Extruded AZ91 Mg Alloys"** in the partial fulfillment of the requirements for the award of the degree of **MASTER OF TECHNOLOGY** and submitted in the **DEPARTMENT OF METALLURGICAL ENGINEERING AND MATERIALS SCIENCE, Indian Institute of Technology Indore**, is an authentic record of my own work carried out during the time period from June 2022 to May 2023 under the supervision of Dr. Hemant Borkar, Assistant Professor , Indian Institute of Technology , Indore .

The matter presented in this thesis has not been submitted by me for the award of any other degree of this or any other institute.

Namrata Sarania
5-06-2023
Namrata Sarania

Signature of the student with date

This is to certify that the above statement made by the candidate is correct to the best of my/our knowledge.

HBorkar

Dr. Hemant Borkar
Supervisor of M.Tech thesis

Namrata Sarania has successfully given her M.Tech. Oral Examination held on **25-05-2023.**

HBorkar

Dr. Hemant Borkar
Assistant Professor, IIT Indore
Date: 2.06.2023

Convenor, DPGC
Dept. of MEMS
Date:

M. Jayaprakash

Dr. Jayaprakash Murugesan
Associate Professor, IIT Indore
Date: 30.05.2023

Abhijit Ghosh

Dr. Abhijit Ghosh
Assistant Professor, IIT Indore
Date: 30.05.2023

ACKNOWLEDGEMENTS

I would want to convey my heartfelt gratitude to Dr. Hemant Borkar, my mentor, for his invaluable advice and support in completing my project. This endeavour would not have been possible without his help and supervision. I could not have asked for a finer mentor in this M.Tech project.

My sincerest gratitude to my PSPC members Dr. Jayaprakash Murugesan and Dr. Abhijit Ghosh for taking time to assess my work and utilize their immense knowledge to provide constructive criticism and suggestions for obtaining the desired results to achieve the said objectives. I am grateful to the Head of Dept., Dr. Ajay Kumar Kushwaha , Dr. Sumanta Samal (Convenor, DPGC) and Dr. Vinod Kumar (Associate Professor, Former HOD, Dept. of MEMS) for allowing me to utilize the various academic resources and department facilities.

I would like to thank Mr. Ankush S. Marodkar and Mr. Hitesh Patil who have given their full effort in guiding and helping me in every step. The completion of the project would not have been possible without their help and insights.

I am grateful to IIT Indore for providing the necessary resources for research.

And lastly, I would also like to thank my friends and parents for their support and encouragement as I worked on this project.

With regards,

Namrata Sarania

Abstract

In this work, calcium, strontium, and cerium were introduced as alloying elements to the AZ91 alloy, which served as the base material. It was discovered through microstructural research using an optical microscope (OM) and a field emission scanning electron microscope (FESEM) that the AZ91 base alloy has an interdendritic network of β -$Mg_{17}Al_{12}$ and a magnesium matrix. The dispersion of the interdendritic network was more evenly distributed in the corresponding squeeze cast AZ91 alloys as a result of the addition of individual calcium, strontium, and cerium. Ca, Sr, and Ce additions resulted in the refinement of the secondary phase ($Mg_{17}Al_{12}$) in the microstructure. Ce addition creates a new rod-like phase known as $Al_{11}Ce_3$, Ca addition creates a skeleton-like structure of β -$Mg_{17}Al_{12}$, and Al_2Ca while Sr addition creates bright needle-like structures of Al_4Sr intermetallics. The volume percentage of β -$Mg_{17}Al_{12}$ was significantly reduced with individual Ca, Sr, and Ce additions and combined additions of Ca and Sr due to the production of new Al_2Ca, Al_4Sr and $Al_{11}Ce_3$ intermetallics. The average grain size was found to be reduced with individual Ca, Sr, and Ce additions, as seen by the grain size calculated from Electron Backscatter Diffraction (EBSD) maps. There are certain differences in the tensile properties like yield strength , ultimate strength and elongation of the AZ91 alloy and it was discovered that adding these components improved its hardness. The extruded AZ91 alloy's inclusion of Ca and Sr reduces grain size and yields asymmetry. As a result, extruded AZ91-Ca -Sr alloy's mechanical properties have improved. Overall, the findings of this study show the potential for individually adding calcium, strontium, and cerium as well as merged additions of calcium and strontium as alloying elements to cast and extruded AZ91 alloy in order to modify its microstructure and enhancing its mechanical properties.

TABLE OF CONTENTS

LIST OF PUBLICATIONS

- **Namrata Sarania**, Ankush S. Marodkar and Hemant Borkar, "**Influence of Ca and Ce Additions on Microstructure and Microhardness of Squeeze-cast AZ91 Mg Alloy**". Submitted to '**Materials Science Forum'**. (Status – Under Review)

LIST OF FIGURES

LIST OF TABLES

ACRONYMS

HCP : Hexagonal Close Packed structure

FCC : Face Centred Cubic

CRSS : Critical Resolve shear Stress

OM : Optical Microscopy

FE-SEM : Field Emission Scanning Electron Microscope

EDS : Energy Dispersive X-Ray Spectroscopy

XRD : X-Ray Diffraction

EBSD : Electron Backscatter Diffraction

SDAS : Secondary Dendrite Arm Spacing

AGS : Average Grain Size

EDM : Electric Discharge Machine

DI: De-Ionized

UTM : Universal Testing Machine

ASTM : American Society for Testing and Materials

UTS: Ultimate Tensile Strength

TYS : Tensile Yield strength

CYS: Compressive Yield strength

UCS: Ultimate Compressive strength

ED : Extrusion direction

PSN :Particle Stimulated Nucleation

Fig. : Figure

Et al.: et alia

Chapter 1

Introduction

Due to their high specific strength, which results in significantly better fuel efficiency and less emissions, the use of magnesium (Mg) alloys in the automotive sector has grown considerably over the past few years [1]. Aluminium bearing magnesium alloys (Mg-Al alloys) dominate usage among the variety of magnesium alloys due to their low price and superior castability. It is widely accepted that one of the most vital methods to enhance the mechanical characteristics and workability of cast metal products is through grain refinement [2]. Magnesium, which has a low density as a primary benefit, is used extensively in the automotive sector to address this issue. The potential weight savings due to an increase in magnesium use has major environmental benefits, including a reduction in greenhouse gas emissions, as magnesium has a density that is almost two thirds that of aluminium. The growing need for sustainable engineering solutions has fueled the rising demand for lightweight materials. Magnesium alloys have the ability to help achieve these goals, and this promise has been recognised by sectors like automotive, aerospace, electronics, and medicinal. Researchers and engineers are investigating the use of magnesium alloys in various structural and functional components in the goal of fuel efficiency, lower emissions, and greater performance. Utilising magnesium alloys to their full potential and overcoming the difficulties connected with their use requires a thorough understanding of their fundamental properties, production methods, and application areas. Because magnesium can be recycled, unlike many polymers, it also offers a solution for other global environmental issues including reusability and recycling [3].

1.1 Basics

Magnesium's hexagonal crystal structure has 1.6236 c/a ratio , which is almost close to the spheres' ideal atomic packing value of 1.633 [3]. The high mechanical characteristics of magnesium alloys make them suitable for a variety of engineering applications. Magnesium alloys have a high specific strength and stiffness combination that allows them to bear heavy loads without losing structural integrity. Furthermore, magnesium alloys are easily machined, making it possible to create intricate shapes and patterns. Magnesium alloys are especially appealing for weight-conscious industries like automotive and aerospace thanks to these mechanical qualities.

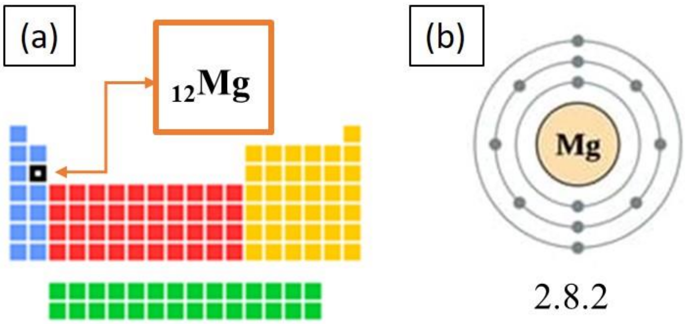

Fig.1.1:(a) Periodic table showing Mg, (b) Atomic structure of Mg

As a result of rapid development of science and technology, numerous series of magnesium alloys have been gradually exploited to satisfy the demands of diverse fields. Due to their affordable cost and moderate mechanical strength, Mg alloys from the AZ group are frequently utilised in manufacturing processes. The Mg-Al series alloys, including AZ91 alloy, are the most successfully created and commonly used magnesium alloys in the AZ series due to the combination of good mechanical qualities and widespread casting [2]. While AZ91 offers an excellent balance of mechanical characteristics, corrosion resistance, and castability, it is not recommended for usage above 120 ◦C due to low creep resistance and a loss in strength at high temperatures. There has been a lot of work put into finding alloying components that are more effective at enhancing high temperature mechanical qualities while being less expensive. According to recent research, adding calcium to Mg-based alloys had the effect of changing the alloys' as-cast microstructure and increasing their mechanical characteristics at both room temperature and higher temperatures [4].

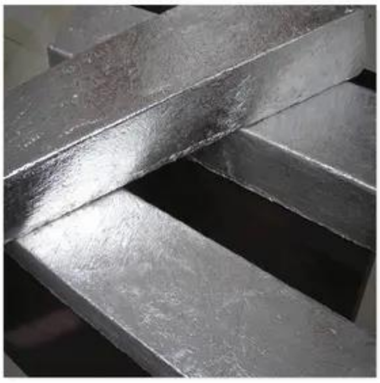

Fig.1.2: AZ91 magnesium alloy blocks

The most common form for enhancing Mg-Al alloys' strength by microstructure refinement is alloying. It has been observed that the alloying addition enhances the nucleation sites during the solidification process in order to produce thermally stable precipitates with Al and Mg predominantly at the grain boundaries, [5]. This results in secondary phases and a more refined microstructure in the Mg-Al alloy. These thermally stable precipitates efficiently stop grain boundary dislocation and migration even at higher temperatures. Therefore, up to a certain point, alloying additions might lead to increased strength [5-7]. A desirable combination of strength, lightness, resistance to corrosion, thermal conductivity, and castability can be found in the robust magnesium alloy AZ91. Because of its characteristics, it is highly sought-after for a variety of applications, including automobile parts, aeronautical structures, electronic gadgets, and athletic goods. It has insufficient creep resistance and only moderately good ductility at normal temperature. Numerous methods, such as alloying with other elements and heat treatment procedures, have been devised to address these drawbacks. The tensile strength, ductility, and creep resistance of the alloy are all improved by these changes. Research and development efforts are still being made to find ways to improve the alloy's performance and broaden its use in different industries [8].

Ca can be added to particles to enhance their quality, disperse them, and change dendritic-shaped particles into rounder, uniformly dispersed small particles. The inclusion of Ca improves the high-temperature properties of magnesium alloys while also promoting hot tearing. However, adding Ca also stops the oxidation and ignition of the melting magnesium alloy and works effectively enough to do so. [1,4,9]

The mechanical and casting properties of the AZ91 alloy are enhanced by the addition of strontium. Strontium works as a grain refiner and modifier when added to AZ91, resulting in a finer and more uniform grain structure. The alloy's mechanical strength, ductility, and fatigue resistance are improved by this refining. Additionally, the use of strontium lowers shrinkage and porosity problems during the casting process, improving casting quality and lowering the amount of scrap produced. To achieve its optimal characteristics it's essential that one carefully limit the amount of strontium added, as too much of it might have a negative impact on how well the alloy performs [6].

Rare earth elements have the power to refine the grains and purify the alloy, which can enhance the mechanical qualities of alloys based on magnesium and aluminium [10]. Particularly when it comes to fortifying Mg alloys, rare earth metals can exhibit distinctive features due to the uniqueness of the electrons in the outer orbit [11]. Rare earths can refine grain, decrease the fraction of the β -$Mg_{17}Al_{12}$ phase, produce intermetallic compounds with rare earths, such as $Al_{11}Ce_3$ in AZ91 Mg alloy, and can directly alter grain size and microstructures of AZ91 Mg alloy, according to studies performed by Cai Huisen et al. [12].

The β -$Mg_{17}Al_{12}$mostly precipitates at the grain boundaries (GBs) during gravity die casting (GC). These β -$Mg_{17}Al_{12}$precipitates operate as crack-nucleation sites when they are mechanically deformed because they are naturally brittle. As a result, the bulky secondary β -$Mg_{17}Al_{12}$phase precipitation at GB degrades the mechanical characteristics of AZ91 [6]. The squeeze casting procedure can alleviate this issue. The secondary β -$Mg_{17}Al_{12}$ coarser precipitates are reduced by the squeeze casting process, resulting in a homogeneous and refined network of -phase. As a result, better mechanical properties may be attained [6].

Gravity and pressurised casting are combined in the process known as squeeze casting. Molten metal is often put into a heated die. A ram is used to gradually provide high pressure to the molten metal head once filling is finished. This pressurisation helps to minimise shrinkage and micro shrinkage porosity by ensuring that metal flows throughout the solidifying casting. This procedure can result in a very fine microstructure when coupled with a controlled cooling stage. It is possible in some circumstances to produce mechanical qualities that are similar to those forged parts. The reduced porosity and fine microstructure significantly enhance the casting's mechanical characteristics and pressure tightness [13].

1.2 Crystal Structure of Magnesium:

When compared to high-symmetry face-centered cubic metals like aluminium and copper, the deformation behaviour of this material is significantly more complex because of its low symmetry crystal structure. (0001) is its close-packed plane, and the close-packed direction is $<11\bar{2}0>$. At room temperature, basal slip is the main process for deformed magnesium and similar alloys. However, it only provides two separate slip systems, which are insufficient to allow for the plastic deformation of each of the to accept the necessary shape change.

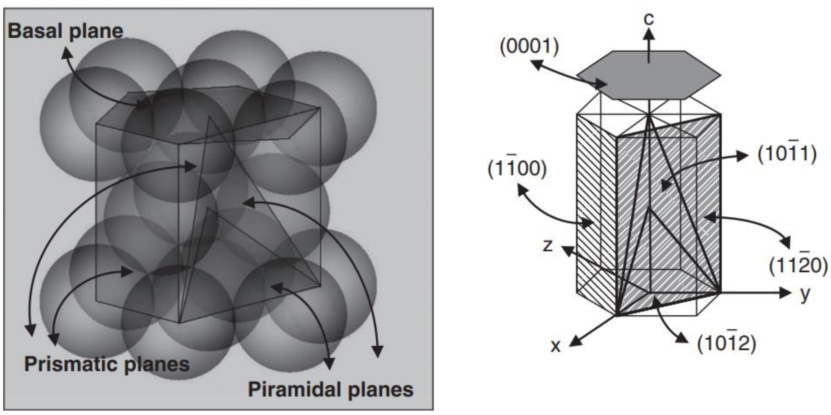

Fig.1.3: Major planes and hexagonal close-packed (HCP) crystal structure of magnesium are shown schematically [14].

Fig. 1.3 depicts the main planes of magnesium and the HCP crystal structure. Lattice parameters of 3.18 A and 5.19 A, which are somewhat below the ideal c/a ratio of 1.62354 of the magnesium crystal at room temperatures, appear significant in explaining several fundamental properties of the metal [14].

Table 1: Comparing the CRSS values for basal planes and c/a ratios of several HCP metals

Metal	CRSS (psi)	c/a ratio
Mg	63	1.624
Cd	82	1.886
Zn	26	1.856
Ti	16000	1.588
Be	5700	1.586

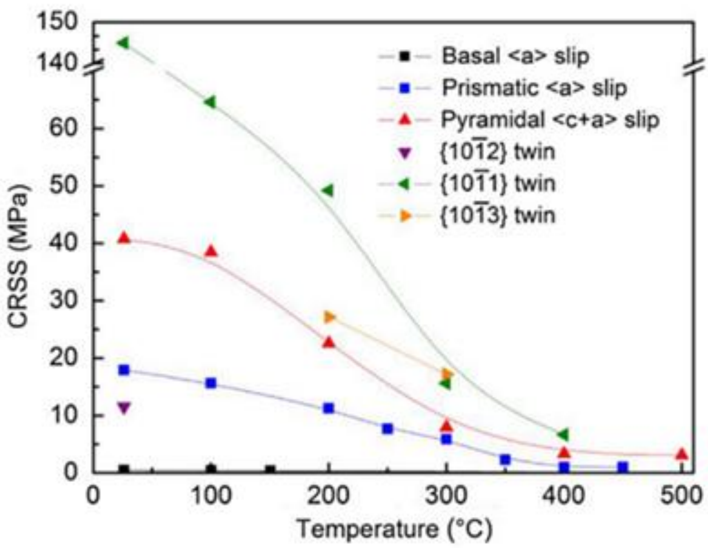

Fig.1.4: The effect of temperature on CRSS values for various slip and twinning modes [15].

At ambient temperature, the CRSS value for activating basal slip in pure magnesium is significantly lower than for prismatic and pyramidal slip. The {10$\bar{1}$2} twins are simpler to activate than the {10 $\bar{1}$1} and {10 $\bar{1}$3} twins. While nearly temperature independent for basal slip, the CRSS value drastically decreases with increasing temperature for other deformation types [15]. At warm to high temperatures, magnesium and its alloys are thermo-mechanically treated to increase the number of deformation modes and hence promote plastic deformation. When magnesium alloys are thermomechanically treated, alloying additives can change the recrystallization texture and change the CRSS values for various slip and twinning modes, which can affect plastic deformation.

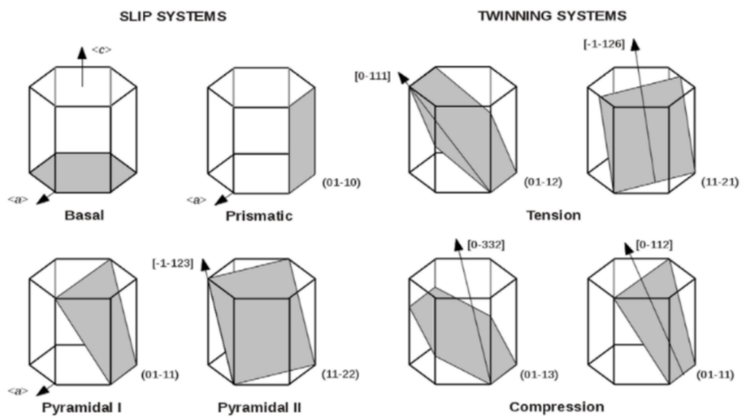

Fig.1.5: Deformation modes in Magnesium[15].

The following Table 2 provides a list of the potential slip modes, their related slip planes, slip directions, computed rotation axis, and number of deformation modes in a hcp crystal structure.

Table 2: Slip systems in HCP materials

Type	Plane	Direction	Rotation Axis	Number of deformation mode	
				Total	Independent
Basal	$\{0001\}$	$\langle 11\bar{2}0\rangle$	$\langle 10\bar{1}0\rangle$	3	2
Prismatic	$\{10\bar{1}0\}$	$\langle 11\bar{2}0\rangle$	$\langle 0001\rangle$	3	2
Pyramidal -I	$\{11\bar{2}0\}$	$\langle 11\bar{2}0\rangle$	$\langle 10\bar{1}2\rangle$	6	4
Pyramidal -II	$\{11\bar{2}2\}$	$\langle 11\bar{2}3\rangle$	$\langle 10\bar{1}0\rangle$	6	5

1.3 Advantages of Mg alloy

The advantages of magnesium alloys are numerous. The key characteristics of magnesium alloys that make them more desirable to the automotive, aerospace, and other industries are shown in Figure. Magnesium alloys have the highest specific stiffness and strength of any structural material since they are the lightest. Other significant advantages include high castability and machinability. Alloys like AZ9l, AM50, and AM60 are the common magnesium die-casting which can be used to make larger, more intricate patterns with thinner sections. As a result, they make it easier to create big die cast components than in a single-shot die casting ,combine structural features that would normally be accomplished through the combination of several small pieces over the course of numerous manufacturing processes.

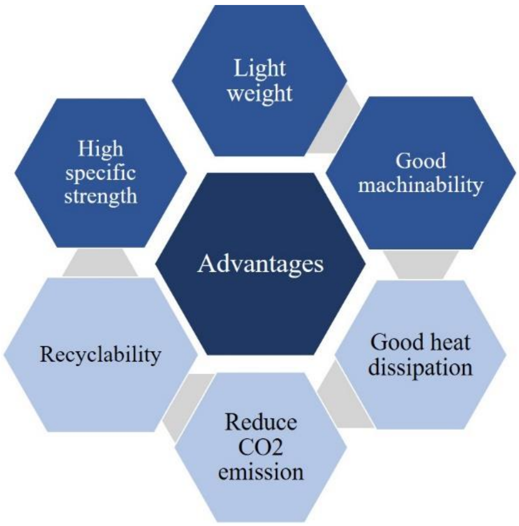

Fig. 1.6: Advantages of Mg alloys

Magnesium alloys, whether cast or wrought, provide outstanding strength-to-weight ratios for a variety of engineering projects. Magnesium alloys are used in a variety of industries, including the automotive, defence, electronic, aerospace, biomedical, manufacturing, and green energy technologies[16]. They are also simple to work with, having the highest known damping capacity of any structural metal, and are up to almost 70% lighter than stainless steel and a third lighter of that aluminium.

Magnesium alloys are essential in situations where components and machinery must be lightweight because they provide designers and material researchers with attainable, high-performing solutions to the age-old challenge of optimising strength, power , weight and cost. Magnesium alloys in particular include:

Lightweight - Magnesium is the lightest structural metal currently available, having a density of 1.7g/cm3. Its alloys are therefore perfect for projects where weight is a top priority, providing a weight advantage of up to 50% over titanium and 33% over aluminium. The transition to electric and energy-efficient automobiles, in particular, will increase demand for component parts to be made lighter and lighter.

Plentiful - Magnesium is a cheap and easily accessible option because it is the eighth most abundant element on earth and the third-most used non-ferrous casting material is magnesium alloys.

Strength - Magnesium's hexagonal, densely packed crystal structure naturally offers high levels of stiffness. Cast magnesium alloys can withstand tensile strength up to 280 MPa and can yield up to 160 MPa, while wrought magnesium alloys can withstand tensile strength up to 360 MPa and can yield up to 300 MPa.

Simple to cast and manufacture -It is able to be injection-molded. Magnesium alloys are useful for enhancing any project's post-life green credentials because they pose no toxicity risks.

1.4 Limitations of Mg alloy

Magnesium alloys have poor formability as a result of a number of factors, such as the creation of strong basal textures during rolling and extrusion and the constrained range of accessible deformation modes resulting from the hexagonal close-packed (hcp) structure of magnesium. At room temperature, magnesium is not very plastic. Its closely packed hexagonal crystal structure at room temperature has just one slip plane and three slip systems, therefore the combined action of slip and twining is mostly to blame for its plastic deformation. With a relatively low equilibrium potential and considerable chemical activity is magnesium. As compared to aluminium alloys, magnesium alloys are more prone to corrosion. Parts manufactured of magnesium alloys may corrode over time, which may result in failures or other problems. Magnesium reacts quickly with oxygen, so it must be kept free of contamination during the fabrication and welding operations to prevent faults or problems in the final product. Additionally, many magnesium alloys require improvement with adequate alloying additions because they have lower strength, particularly in the as-cast form. It is crucial to overcome the significant obstacles associated with Mg alloys in order to have extensive usage of these materials in the automotive and other industries.

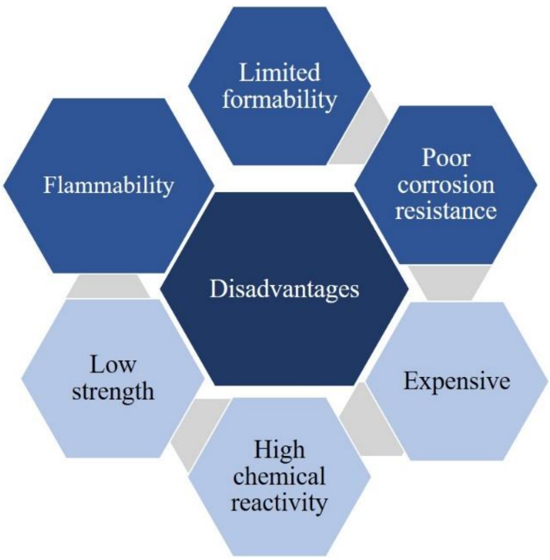

Fig. 1.7: Limitations of Mg alloys

1.5 Application of AZ91 alloy in automobile:

Due to its advantageous characteristics, AZ91 alloy is widely used in the automobile sector for a variety of components. The following are some typical uses of AZ91 alloy in car parts:

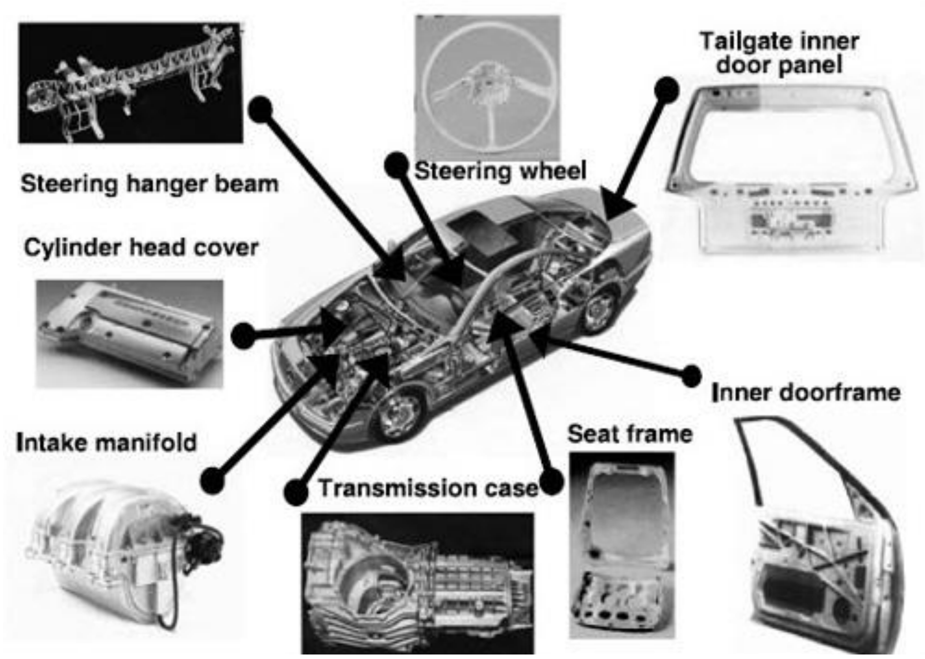

Fig. 1.8: Application of AZ91 Mg alloy in motor vehicles [16].

Engine block: Due to its great strength, lightweight, and superior castability combination, AZ91 alloy is utilised to make engine blocks. The alloy's excellent strength-to-weight ratio helps to retain structural integrity while also enhancing fuel efficiency.

Transmission Cases: Transmission cases are made from AZ91 alloy. Because of its low density, the transmission system is lighter overall, improving fuel efficiency.

Steering components: AZ91 alloy can be used to create steering components including brackets and housings for steering columns. The alloy is a good choice for these crucial components that need to be durable and precise because to its high strength and good machinability.

Suspension components: Control arms and brackets are among the suspension parts that can be produced using AZ91 alloy. The lightweight nature of the alloy minimises unsprung weight, improving handling, ride comfort, and fuel efficiency.

Intake manifolds: Intake manifolds can be constructed using AZ91 alloy. Due to the alloy's outstanding castability, complicated shapes and designs may be created, resulting in optimal airflow and effective engine operation.

Brake callipers: The AZ91 alloy can be used to create brake callipers, which require both strength and heat resistance. The alloy is ideal for these demanding applications because to its high melting point and strong mechanical characteristics.

Wheels: The lightweight quality of the alloy helps in improving vehicle dynamics, including acceleration, braking, and handling.

Chapter 2

Literature Review

The objective of the current study is to give a comprehensive examination of each component of the magnesium AZ91 alloy, which will contribute to a better understanding of this material. Numerous studies have been done on the effects of different alloying elements, such as Sr and Ca, on mechanical property change, texture evolution, and microstructural behaviour. An brief discussion of the alloying elements that are compatible with magnesium is followed by a detailed explanation of how each alloying element affects the characteristics of the material.

Due to its hexagonal crystal structure, which lowers its ability to deform, especially at low temperatures, magnesium has fewer slip systems than FCC aluminium. The majority of deformation takes place at room temperature as a result of twinning on the pyramidal ($10\bar{1}2$) planes and slide on the basal planes in the close-packed <$11\bar{2}0$> orientations. In tension, only pressures perpendicular to the basal planes can cause this type of twinning, whereas only forces which parallel to the basal planes can cause it in compression. More pyramidal ($10\bar{1}1$) slip planes become prominent above around 250 °C, which facilitates deformation and lessens the significance of twinning. Hot working is therefore frequently employed to create magnesium alloy products. The production of w materials, which now only make up around 1% of magnesium use, mostly involves rolling, extrusion, and press forging at temperatures between 300 and 500 °C [15]. Extrusion speeds are five to ten times slower than what is feasible with aluminium alloys, and rolling is typically required to be done in several stages.

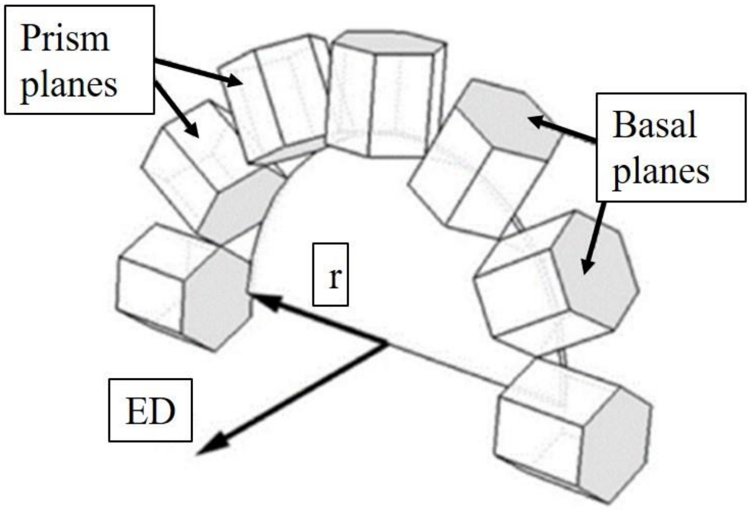

Fig.2.1: The relationship that exists between the basal and prismatic planes in the texture of the basal fibre resulting from extrusion. Extrusion direction is ED, while radial direction is r [24].

2.1 Alloys based on Mg- Al, Mg-Zn, Mg-Zn-RE system

2.1.1 Alloys based on the magnesium–aluminium system: The most extensively used magnesium casting alloys are based on the Mg–Al system. The majority of alloys comprise 8–9% aluminium with tiny amounts of zinc, which increases tensile qualities, and manganese, such as 0.3 percent, which improves corrosion resistance. In alloys containing more than 2% aluminium, the phase $Mg_{17}Al_{12}$ exists in the as-cast condition. Although adding zinc to Mg–Al alloys strengthens them, the amount of zinc added is limited due to an increase in susceptibility to hot cracking during solidification [15]. Cast Mg–Al and Mg–Al–Zn alloys show some susceptibility to microporosity but otherwise have good casting qualities and resistance to corrosion is generally satisfactory.

2.1.2 Magnesium- Zinc based alloy: Zinc strengthens solid solutions more than aluminium at the same atomic percentage, but its solubility is substantially lower. In Mg–Zn alloys, minor additions may alter precipitation. Calcium and strontium, for example, speed up the rate of ageing while delaying overaging, refine the sizes, and increase the number of densities of precipitates that occur [15].

2.1.3 Magnesium-RE-Zinc alloys: The development of Mg-RE-Zn alloys for high temperature applications has been made because Mg-Al and Mg-Zn-based alloys have a poor creep resistance. The tensile characteristics and creep resistance of die cast magnesium-resin alloys are significantly influenced by the choice of RE elements.

2.2 Role of alloying element

Surface active elements like Sb, Ca, Bi, Sr, RE, etc. are added to the AZ91 alloy to improve its mechanical characteristics and microstructure. The majority of the time, these elements mix with magnesium or aluminium to create alloys that are more thermally stable than $Mg_{17}Al_{12}$ and so have better creep qualities. Several elements, including Ca and Sr, can assist refine the AZ91 alloy's grain size. It is also found that adding Ca and RE, as well as Sr and RE, improves the mechanical properties and grain refinement of the AZ91 alloy.

2.2.1 Calcium:

Wang Qudong et al. [17] studied the microstructure and mechanical properties of the AZ9l alloy after adding up to 2% Ca. Ca addition was discovered to enhance the microstructure and lessen the presence of β - $Mg_{17}Al_{12}$ phase by producing a new Al_2Ca phase. The inclusion of Ca can aid in reducing AZ9l particle size. According to Hirai et al.[4], the initial grain size of as-cast AZ9l alloy decreases from 65 um to 20 um with the addition of 1% Ca. When the increased calcium content exceeds 1%, no difference in particle size is seen.

The inclusion of Ca improves the yield strength at room temperature, but it reduces the ultimate tensile strength and ductility. However, the Al_2Ca phase that forms at grain boundaries has a brittle, face-centered cubic structure that could reduce the bond strength and aggravate UTS and elongation. This is despite the fact that the grain refining action of Ca is credited with enhancing yield strength. Additionally, with the addition of Ca, an increase in the stability of the intermetallic $Mg_{17}Al_{12}$ is seen.

2.2.2 Rare earth:

A rod-like $AI_{11}RE_3$ intermetallic forms at the grain boundary when rare earth elements are added. The amount of Al available for the creation of the $Mg_{17}Al_{12}$ phase decreases as a result of $AI_{11}RE_3$ production. The literature on the impact of RE addition on the tensile characteristics of AZ9l alloy is inconsistent. According to Y. Lu[18], RE significantly increases the tensile strength and elongation at high temperatures but has no impact on the UTS of AZ9l at room temperature. Fan asserted that the AZ9l alloy's ductility and UTS were both noticeably improved by the inclusion of La and Ce. However, G. H. Wu et al.[19] found that while the UTS enhanced but the elongation dropped as RE additions increased. Improved corrosion behaviour was discovered by Fan et al.[18] after studying the impact of Ce and La inclusion on the corrosion behaviour of AZ9l alloy.

2.2.3 Strontium :

The changed precipitation behaviour seen with Sr addition is responsible for the grain refining. The $Mg_{17}Al_{12}$ phase precipitates more frequently along the grain boundary with Sr addition, it is discovered. K. Hirai et al.[4] found that 0.5% Sr to AZ91 alloy only resulted in a grain reduction of 65 um to 40 pm. The grain size was also significantly reduced to 17 um when it was treated with 1% Ca. As a result of the decreased stacking fault energy, it is also claimed that the combined addition of Sr and Ca enhances the characteristics at low and high temperatures. By adding 0.5% Sr to the AZ91 alloy, S. Lee et al.[20] did manage to achieve low hardness and fracture toughness. This is due to the presence of both massive, needle-shaped Sr-based precipitates, which are primarily found on grain boundaries, as well as discontinuous $Mg_{17}Al_{12}$ precipitates. These particles first form microcracks when load is applied, but these cracks quickly join to grain boundaries and produce intergranular facture. As a result, despite the low grain size, it has weaker mechanical properties.

2.3 Influence of alloying elements on Mg alloy

The strength and rate of degradation of as-cast magnesium are both high. The material properties can thus be improved by using the proper alloying and processing processes. Magnesium is a chemically reactive element that interacts with chemicals used in alloying to form intermetallic compounds. The intermetallic phases found in magnesium alloys have an impact on the their microstructure, that affects the material characteristics. The alloying elements strengthen solid solutions, refine grains, and precipitation harden materials to rapidly increase mechanical properties.

Table 3: Influence of some alloying elements on Mg alloy

Alloying element	Influence on material properties of Mg alloy
Aluminium	improves castability, strength, and hardness
Calcium	increases the effectiveness of grain refining, creep resistance, and corrosion resistance.
Cerium	decreases yield strength while increasing elongation and work hardening rate.
Iron	negatively affects corrosion resistance
Lithium	reduces strength and improves ductility
Manganese	enhances resistance to salt water corrosion
Strontium	refines the grain and improves creep and corrosion resistance. improves bone mass.
Zinc	Increased yield stress and better corrosion resistance
Zirconium	very good grain refiner

Silicon	Enhances fluidity
Nickel	Improves mechanical property
Yttrium	enhances resistance to high temperatures

2.4 Findings and shortcomings in literature :

According to research by Wang Qudong et al. [17], adding Ca can change the microstructure of the AZ91 magnesium alloy, reduce the amount of β -$Mg_{17}Al_{12}$ phase, and produce new Al_2Ca phase. The addition of Ca reduces the tensile strength and elongation of the AZ91 magnesium alloy at room temperature, however the addition of Ca to the alloy results in elevated temperature strengthening. The ideal addition of Ca and Sr to the AZ91 magnesium alloy in order to achieve outstanding mechanical properties at both room temperature and increased temperature was studied by Kinji Hirai et al. [4]. Microstructural tests were carried out to establish the ideal concentrations of additional components. According to Shang et al. [21], the addition of Ca to magnesium proved successful in refining grains. Ca, in modest quantities, can improve mechanical characteristics and microstructure.

Since grain refinement is essential for producing high-performance Mg-Al alloys, S.F. Liu et al. [1] reviewed preliminary research that has focused on the influence of the addition of Ce combined with Ca or Sr on the microstructure refinement of AZ91 magnesium alloy. The Al 4Sr intermetallic decreases the volume percentage of the phase and enhances tensile characteristics, as demonstrated by Aria Afsharnaderi et al. in their study [22]. With different Ca contents of 1, 2, and 3 wt%, Yang Zhang et al. [9] conducted grain refinement investigation of Ca addition on AZ91 alloy. The alloys were called AZX911, AZX912, and AZX913, respectively. Additionally, they investigated how the squeeze casting alloy AZX912's microstructure and mechanical characteristics were affected by the pressure that was applied. In this work, it is examined how squeeze casting AZX912 alloy's microstructure and mechanical properties are affected by applied pressure (from 0 to 120 MPa, Fig. 2.2).

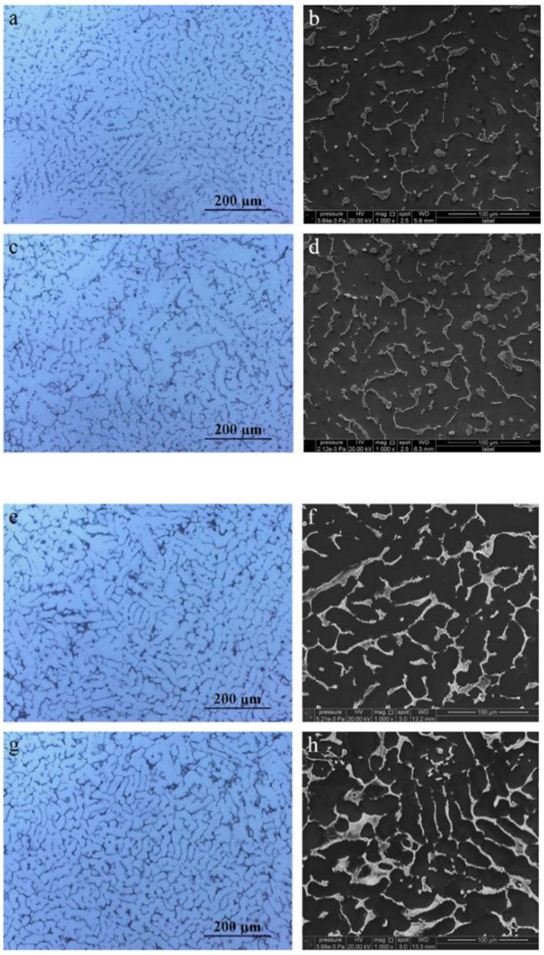

Fig.2.2: Analysing the change in microstructure at constant temperature (at 700 °C) and applied pressures of 0 MPa, 40 MPa, 80 MPa, and 120 MPa, respectively [9]

It can be seen that the AZX912 alloy's as-cast microstructure is made up of α-Mg dendrites and eutectic dispersed throughout the matrix. When pressure is applied, the microstructure refinement is readily visible. As applied pressure is increased, dendrites get smaller and dendritic arm spacing reduces. The finest dendrites are discovered at a high applied pressure of 120 MPa.

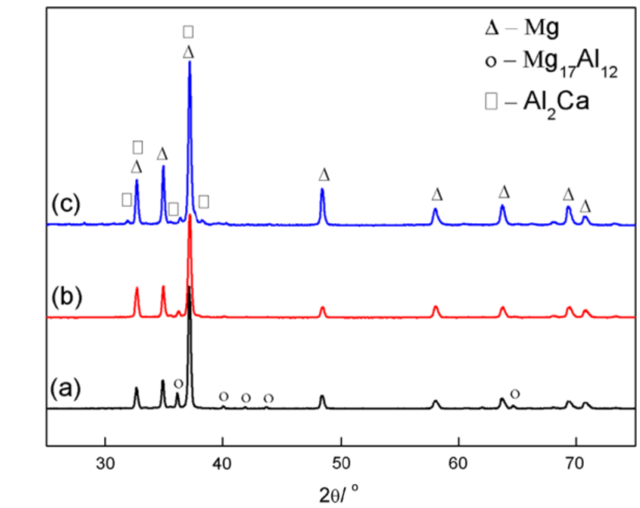

Fig.2.3: Squeeze-cast AZ91-Ca alloys with various Ca concentrations, as seen in their XRD patterns[9]

The AZ91-Ca alloys investigated in this article are composed of α-Mg, β -$Mg_{17}Al_{12}$, and Al2Ca phases, although the proportions of these phases change depending on the quantity of Ca present. As seen in Fig. 2.3, the primary phases of the AZX911 alloy are α -Mg and β -$Mg_{17}Al_{12}$. Al_2Ca's diffraction peaks are too weak to be seen. The amount of β -$Mg_{17}Al_{12}$ phase in AZX912 alloy drops and the amount of Al2Ca phase increases when the Ca concentration rises from 1 wt% to 2 wt%. The amount of β -$Mg_{17}Al_{12}$ phase drops further as the Ca concentration rises to 3 wt%, whereas the amount of Al_2Ca phase dramatically increases.

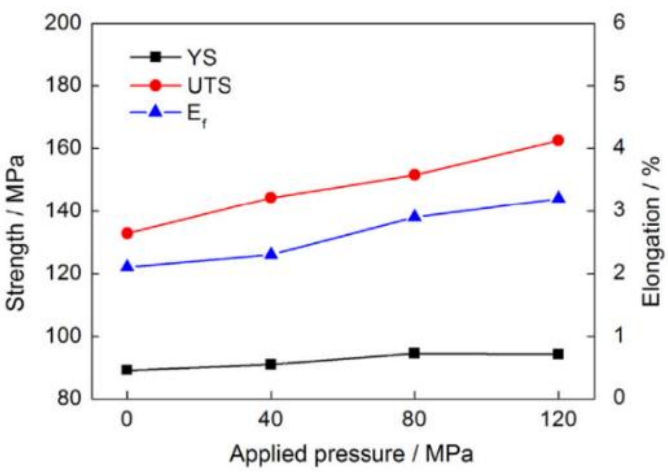

Fig.2.4: Effects of applied pressure on YS, UTS, and Ef of squeeze casting AZX912 alloy (Ca content 2 wt%) [9].

Increasing applied pressure has been proven to improve yield strength (YS), elongation to failure (Ef), and ultimate tensile strength (UTS). The ideal mechanical characteristics can also be found at the highest applied pressure. In the AZX912 alloy squeeze cast at 120 MPa, YS, UTS, and Ef are 94.4 MPa, 162.5 MPa, and 3.2%, respectively. These values are 5.7%, 22.4%, and 52.3% higher than the corresponding values of the samples produced without pressure.

There is an optimal quantity of Sr to add, according to Sadeghi A et al. [23]. Too much Sr will result in cracks forming at the Al-Sr precipitates, making the alloy brittle when deformed. According to H.Borkar et al. [24], M1-Sr alloys have weakened texture as a result of the creation of random texture components during extrusion. The textural randomization is caused by particle stimulated nucleation (PSN) that takes place during recrystallization close to Mg-Sr intermetallics.

(a)

(b)

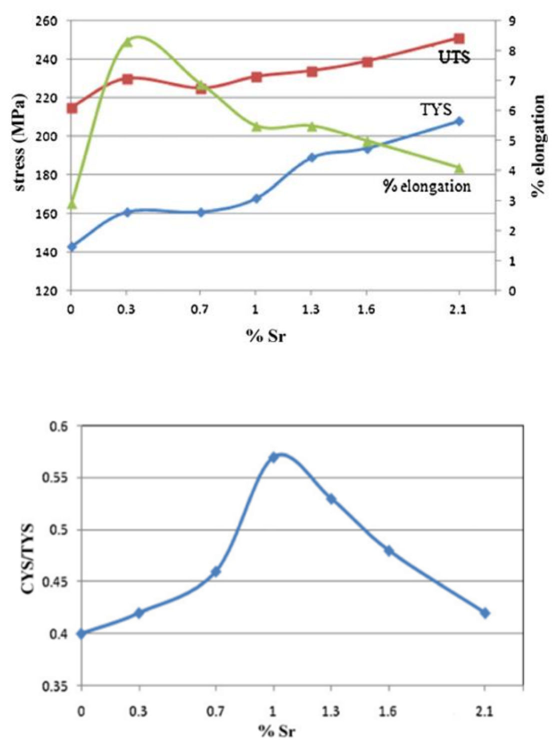

Fig.2.5: (a) Tensile tests in the extrusion direction of high-speed extruded alloys: effect of Sr on mechanical characteristics. Tensile yield stress (TYS) and ultimate tensile stress (UTS) ; (b)Effect of Sr on the yield asymmetry of high-speed extruded alloys (CYS/TYS)[24].

Tensile yield stresses significantly rise with increasing Sr addition, but ultimate tensile stresses increase more gradually. With an initial increase (from 2.9 to 8.3) as Sr increases up to 0.3% addition, followed by a reduction as Sr grows to 2.1%, the elongation (fracture strain) in tension exhibits erratic behaviour. Up to 1% Sr, the yield asymmetry of M1 reduces (i.e., CYS/TYS increases) before rising to 2.1% Sr (Fig. 2.5 (b). With the help of texture weakening, solid-solution strengthening, grain-size reduction, and precipitation strengthening, A. E. Davis et al. [25] focused on the yield asymmetry and anisotropy of wrought magnesium alloy.

The mechanical behaviour and plasticity of Sr-containing AZ31 alloys were studied by K Hazeli et al. [13]. This study provided significant evidence regarding the effects of Sr on the microstructure of Mg extrusion rods, in addition to quantitative and spatially resolved data on the relationships between plasticity and texture and activation of deformation mechanisms, particularly at early stages of plasticity. K. Hazeli et al. [26] investigated that the Al-Sr intermetallic increases particle stimulated nucleation (PSN), according to detailed textural measurements [27,28].

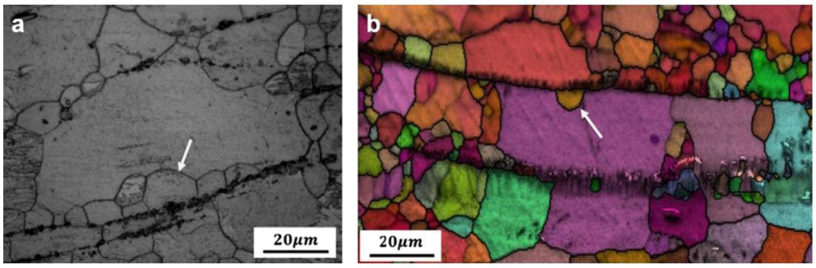

Fig. 2.6: PSN phenomena [29].

It was observed that the recrystallized grains have a different orientation from their parent crystal in Fig. 2.6, where PSN granules at the stringer boundary are seen developing into the parent grain. In AZ31-Sr alloys, Sr induces an efficient process to produce new grains with random orientations, reducing the strength of the strong basal textures [29].

Chaojie Che et al. [30] looked into the microstructures of the AZXSE91100 alloy in both its cast and extruded states. The Mg matrix and intermetallics containing β -$Mg_{17}Al_{12}$, CaMgSi, $Al_{11}RE_3$, Al_2RE, and Mg_2Si make up the microstructure of the AZXSE91100 alloy. The coarse intermatallics were broken up into smaller, more evenly distributed pieces pieces, obviously purifying the DRXed grain.

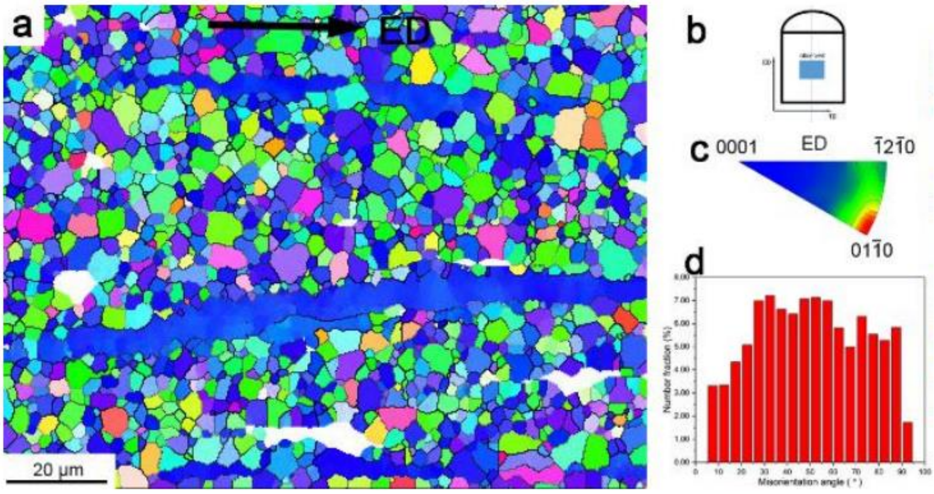

Fig. 2.7: EBSD IPF map and grain distribution [30]

The microstructure of the extruded AZXSE91100 alloy is depicted in Fig. 2.7 (a) having a deformed microstructure with an average grain size of 3.0 μm. The schematic representation of how to collect a sample for EBSD is shown in Fig.2.7 (b). The as-extruded alloy has a strong <0001> texture, as seen by the IPF in Fig. 2.7(c). According to the misorientation angle distribution histogram in Fig. (d), the hot extrusion method produces a significant portion of high angle grain boundaries (>15°, HAGBs).

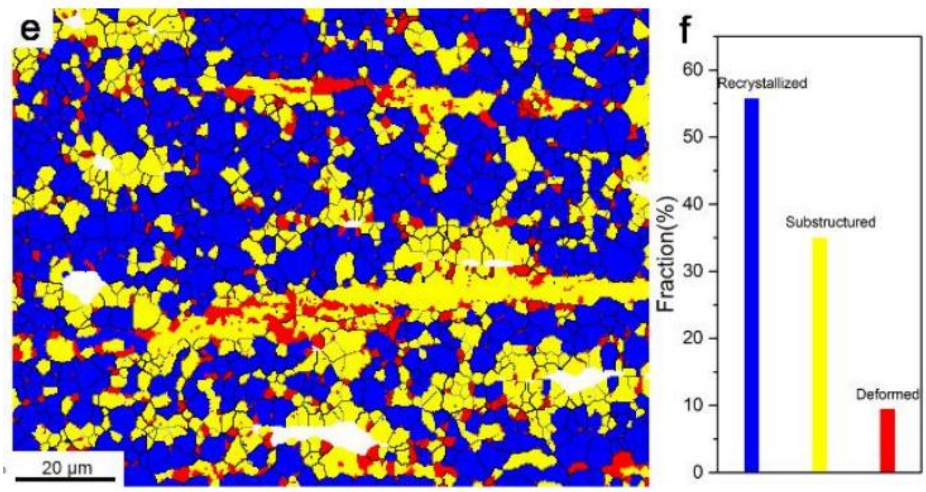

Fig. 2.8: Recrystallized grains and recrystallized fraction [30]

As-extruded alloy sample contains 55.7% recrystallized grains, 34.9% sub-structured grains, and 9.4% deformed grains, as shown by the distribution map of recrystallized grains (Fig. 2.8(e)) and the histogram of recrystallization statistics (Fig. 2.8(f)).

It is widely acknowledged that rare earth elements have the potential to enhance the mechanical properties of Mg-Al based alloys through the effects of alloy purification and grain refinement. Wenxian Huang et al. [31] investigated how the microstructure and mechanical properties of the die-cast AM60 alloy were affected by a modest Cerium addition. According to this study, AM60-1.0Ce alloy achieves the best mechanical qualities; however, as Ce content rises to 1.5%, mechanical properties begin to deteriorate marginally (Fig. 2.9(a)).

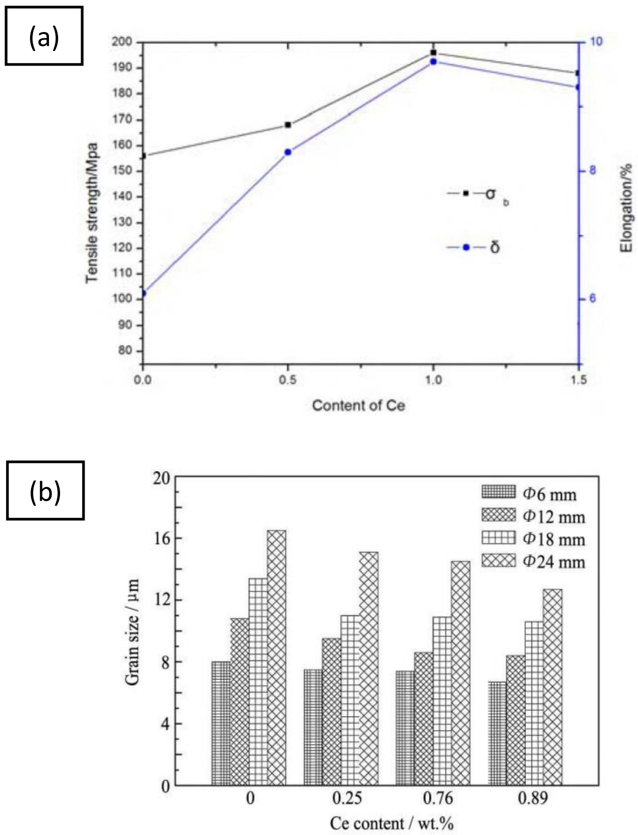

Fig.2.9: (a) Improvement of the mechanical characteristics of the die-cast AM60 alloy after the addition of cerium, (b) The influence of Ce concentrations and solidification rates on grain sizes [32].

Through their investigation, Cai Huisheng et al. were able to demonstrate how Ce could refine grain size, lower the fraction of eutectic β -$Mg_{17}Al_{12}$

phase, generate Al_4Ce phase, and lower the amount of solid Al solution in the α-Mg matrix. Fig. 2.9(b) demonstrates unequivocally how increasing Ce content and increasing solidification rate can both refine grain size [32].

2.5 Summary

There are many literature on individual addition of Ca and Sr, and combined addition of Sr and RE elements to Mg alloys but the combined impact of the alkaline earth elements strontium and calcium on the microstructure refinement and mechanical properties of the as-cast as well as extruded AZ91 alloy has received little attention in earlier literatures. Furthermore, to our knowledge, the influence of the combinative addition of Ca and Sr on the microstructure, mechanical properties, and texture of magnesium alloys has not been systematically studied, which would undoubtedly be more intriguing to research. In this study, the impact of the combined addition of Ca and Sr to the AZ91 alloy as well as each element's solo addition is examined. There are numerous research activities on die-cast AZ91 alloys, this thesis work is focused on Squeeze casting of AZ91 Mg alloy. Additionally , a comparative study on the effect of individual addition of alkaline earth elements (Ca and Sr) and rare earth element (Ce) to AZ91 alloy is investigated.

Chapter 3

Objectives

This work represents an effort to correlate the mechanical behaviour and microstructural features (that includes SDAS, grain size, and volume fraction of interdendritic network) of squeeze-cast AZ91D alloys at room temperature with the addition of Ca and Sr as well as the combined addition of Ca and Sr to AZ91 alloy. Extrusion of the AZ91 alloy (with alloy additions of Ca and Sr) is then done to examine its mechanical properties and texture. Investigations were made into the microstructure and microhardness of the as-cast AZ91 alloy with the addition of 1wt%Ca, 1wt%Sr, and 1wt%Ce. The main objectives of this present work are :

1. To study the effect of Ca and Sr addition on microstructure and mechanical properties of AZ91 Mg alloy after squeeze casting
2. To study the effect of Ca and Sr addition on texture, microstructure and mechanical properties of AZ91 magnesium alloy after extrusion.
   - To optimize Ca and Sr content to improve both texture and mechanical properties after extrusion.
   - To determine the parameters affecting mechanical properties in extruded AZ91-Ca-Sr alloys.
3. To study the individual effect of Ca ,Sr and Ce addition on microstructure and mechanical properties of squeeze-cast AZ91 Mg alloys

Chapter 4

Experimental Work

The primary experimental phases are given in the form of a flowchart below as part of the research methodology for this study.

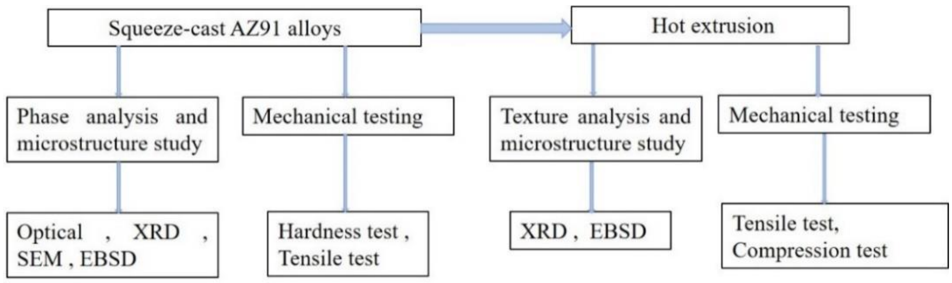

Fig.4.1: Research methodology flowchart

4.1 Casting of alloys

For the preparation of the AZ91-Ca, AZ91-Sr, AZ91-Ce, and AZ91-Ca-Sr squeeze cast alloy samples, the Mg-Ca master alloy (Mg - 20% Ca), Mg-Ce master alloy (Mg - 20% Ce) , Mg-Sr master alloy (Mg-20%Sr) and the AZ91 Mg alloy ingot were used. As a reference, squeezed castings of the unprocessed AZ91 were also used. stir casting machine with a bottom pouring set up was used to produce samples of squeeze cast alloy. This technique involved melting the material in an electrical resistance furnace and pouring it using a bottom pouring device that was coupled to a squeeze casting setup. Fig. 4.4 shows the step-by-step process used to get desired squeeze cast rods , and Fig. 4.2 and 4.3 depicts the setup for a stir casting machine bottom pouring type. The required quantity of AZ91 alloy was placed to the melting crucible following a preheating of the melting furnace at 700 °C. For 60 minutes, the melt was kept at this temperature to ensure full melting. Mg-Ca, Mg-Sr and Mg-Ce master alloys with their estimated amount were added to the melt. The melt was then given 10 minutes to settle down while being stirred consistently at 300 rpm. To prevent oxidation, all procedures were performed in an argon (99.5 vol%) + SF_6 (0.5 vol%) protective atmosphere. For squeeze cast alloys, the bottom pouring arrangement was used to pour the molten metal at 700 °C into a cylindrical cast-iron mould. The mould was preheated to 200 °C using an external heater setup before the melt was poured into it. The mould was then covered with a thin layer of graphite oil. As soon as the pouring operation was finished, squeeze casting at 100 MPa for 30 s was performed to produce squeeze cast rods with diameter 40 mm and length 300 mm . Table 4 displays the list of casting parameters.

Table 4: Squeeze casting parameters

Parameters	Set values
Size of the melting crucible	1200 cm^3
Furnace temperature	700 °C
Melt temperature	700 °C
Pre-heating temperature of the mold	200 °C
Runway temperature	750 °C
Stirrer speed	300 rpm
Stirring time	10 min
Applied pressure	100 MPa

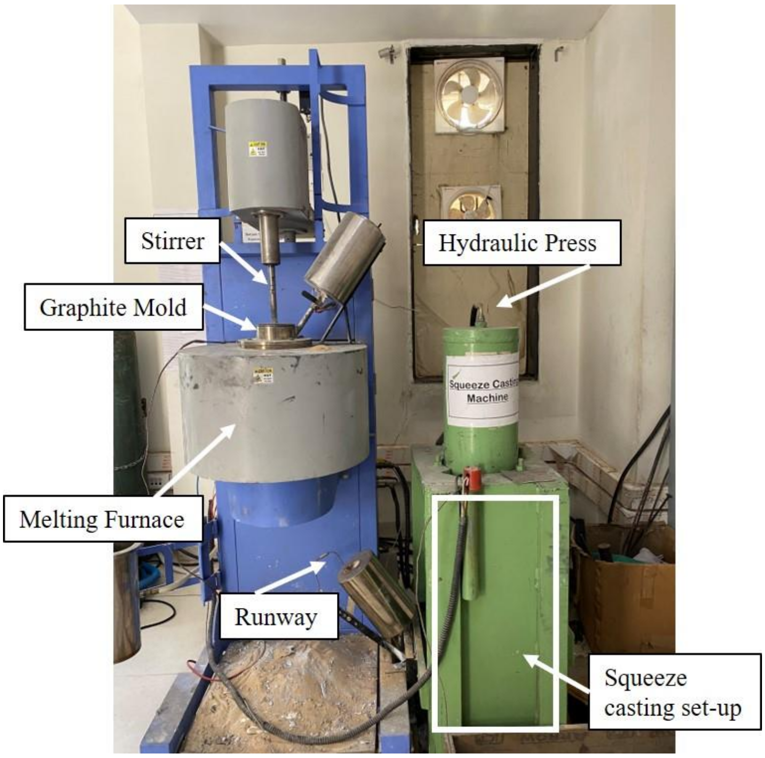

Fig.4.2: Setup for a bottom pouring stir casting machine

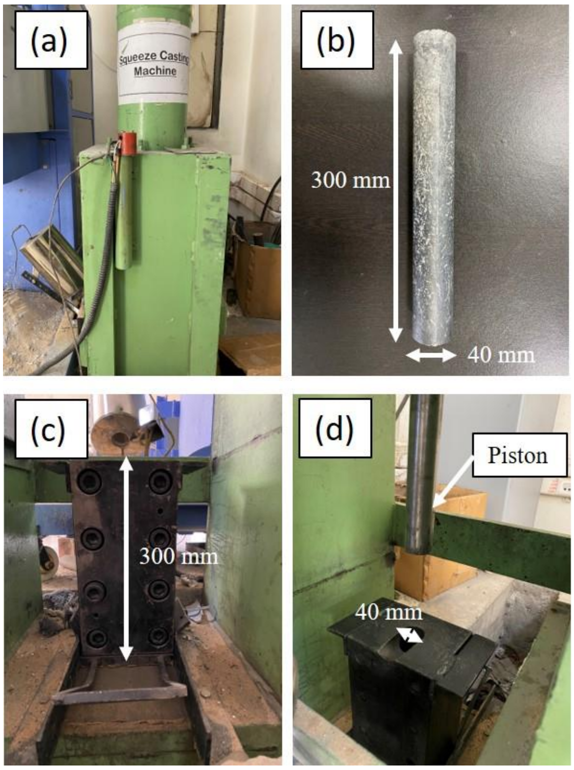

Fig. 4.3: (a)Squeeze cast set up, (b) Obtained squeeze-cast rod with dimension, (c)Squeeze casting die with dimension, (d)Piston

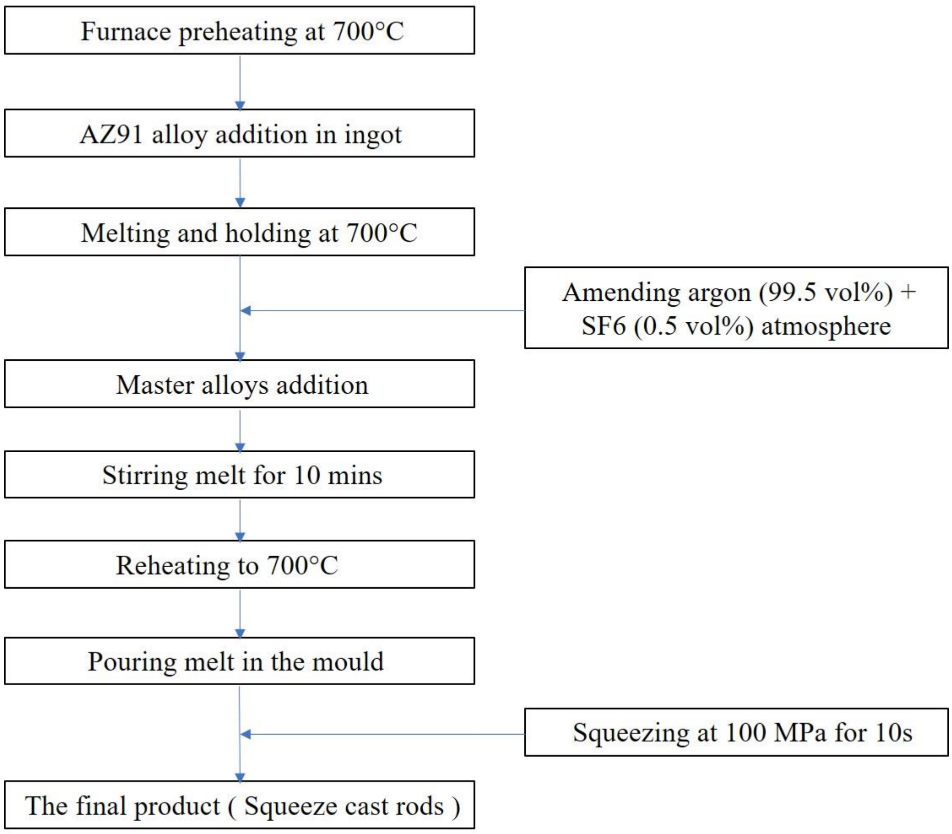

Fig.4.4: Flowchart illustrating the intricate processes used for producing the squeeze cast AZ91 alloys.

Table 5: Obtained cast alloys with their alloy code

Alloy Code	Obtained alloys
X1	AZ91
X2	AZ91-0.3wt%Sr
X3	AZ91-0.6wt%Sr
X4	AZ91-1wt%Ca
X5	AZ91-1wt%Ca-0.3wt%Sr
X6	AZ91-1wt%Ca-0.6wt%Sr

4.2 Hot Extrusion

To manufacture cylindrical extruded bars with a diameter of 20 mm and a length of 250 mm, the extrusion was done at 400°C providing 4:1 extrusion ratio. The temperature was adjusted with the aid of the controller after the thermocouple was put through the container's hole. The activation knob was used to move the ram, and the ram speed could be changed. Once the proper temperature was obtained, the samples were put inside the channel and held there for 1 hr before extrusion was done. After extrusion, the samples were allowed to cool in the open air.

Fig.4.5: Hot extrusion set-up

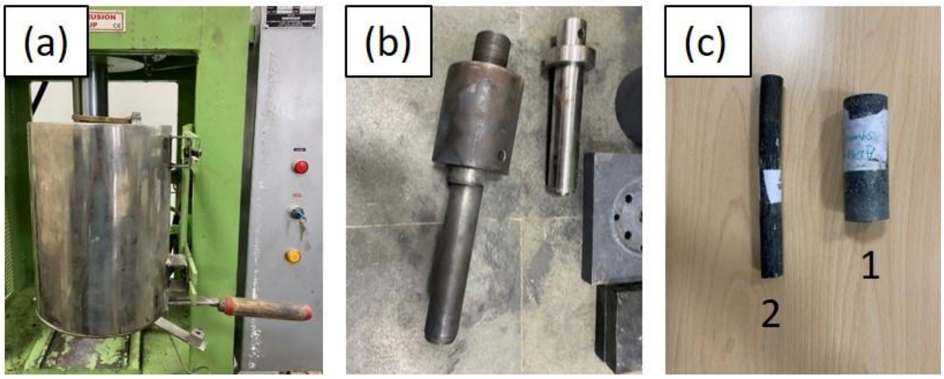

Fig.4.6: (a) Electric furnace, (b)Extrusion punch, (c) Samples before(*1*) and after extrusion (*2*).

4.3 Optical Microscopy

The samples were polished with cloth (up to 1 micron) after being ground with 200- 2500 grit papers. For further optical microstructural analysis, the samples were etched with a 2% nital (for as-cast alloys) or acetic picral (for extruded alloys) solution. The sample was immersed for 2-4 seconds to complete the etching, after which the surface was washed with running water before being dried with a dryer. OM, Zeiss Axiovert A1 inverted microscope was used for microstructural analysis.

4.4 Field Emission Scanning Electron Microscopy (FE-SEM)

Using a JEOL, JSM-7610 F plus the presence of second phases and their morphology in as-cast alloys were investigated. Analysis was done in backscattered mode with a 15kV accelerating voltage. Similar to optical microscopy, the samples for SEM were prepared. Point scans were used to determine the phase compositions using energy dispersive spectroscopy (EDS). Point scan and elemental mapping were used to find the distribution of the phases in the microstructure.

4.5 X-ray Diffraction(XRD)

1cm x 1cm samples were prepared for XRD analysis to identify the peaks of respective alloys and their intermetallics. Panalytical Empyrean XRD Diffractometer was used for the XRD analysis for all the samples.

4.6 Electron Backscatter Diffraction (EBSD)

In order to learn more about the specimens microtexture, EBSD was employed. For EBSD, a JEOL, JSM-7610 F plus was used with a tilt angle of 70°. In order to ensure that enough grains were included in the scan, the proper magnification was employed in consideration of the specimen's grain size. For EBSD, the step size was chosen so that the scan would cover required points, which is necessary to provide scans of high quality. The HKL-2000 software was used to process the EBSD data.

The grains in an extruded sample that have an internal misorientation spread of more than 3° and exhibit a change in colour shade have been classified as deformed or parent grains. Deformed grains were those that displayed uniform colour and had low interior misorientations (less than 3°). Even though the majority of recrystallized grains and malformed grains could be easily distinguished, only a small number of grains in each sample showed interior misorientations that spread closer to 3°. The orientations of the recrystallized grains around the stringers were identified. The effect of having a stringer below the parent would only be to significantly increase the distance along which misorientation exists because the stringers are not in random orientation but are instead aligned in the extrusion direction.

4.7 Mechanical testing

4.7.1 Microhardness testing

A Vickers micro hardness tester (HM 112, Mitutoyo Co.,Tokyo, Japan) was used to conduct Vickers microhardness testing. Six measurements for each sample were taken during the hardness testing process at load 300 g and 20s dwell time, and the average HV was displayed.

4.7.2 Tensile testing

Tensile testing was performed in keeping with ASTM requirements using UTM, Instron 5967 universal testing machine. Figure depicts the tensile testing specimen geometry. Two samples from each as-cast alloy rods were taken for testing, and the average mechanical property values were calculated. The samples were evaluated at room temperature (25 °C) at a strain rate of 0.001 s^{-1}.

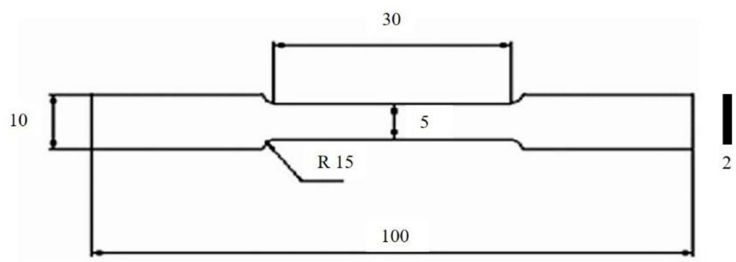

Fig.4.7: Schematic diagram of tensile specimen (all the dimensions are in mm)

4.8 Metallographic preparation

To examine the microstructure of a material using a light microscope, it is necessary to prepare the specimen correctly. The preparation process for light microscopy typically involves several key steps, which include:

- Sectioning
- Grinding and polishing
- Etching

4.8.1 Sectioning

Sectioning is a crucial process that involves two main objectives: creating a specimen cross-section for examination purposes and reducing the size of the specimen to fit on a light microscope stage. To achieve more precise cutting, wire cut EDM is utilized as an electric discharge machine. This type of machine is ideal for sectioning electrically conductive materials. The cutting process involves an electric discharge between an electrode, which is typically a metallic wire, and the specimen immersed in a dielectric fluid. By programming the wire EDM machine, the electrode can be used to cut a predetermined contour in the workpiece. To successfully section the specimen, it must be appropriately positioned in the specimen holder. During the machining process, each discharge generates a crater in the workpiece, removing material, and affecting the tool. The solidified material along the machining path must be meticulously removed in further preparation procedures.

4.8.2 Grinding and polishing

Grinding is an essential process that involves flattening the surface of the specimen to be examined and eliminating any damage resulting from sectioning. To achieve this, a sequence of abrasives with increasing fineness is utilized, starting with a coarse grit. Abrasive paper is categorized according to the size of the abrasive particles, such as 180, 220, 400, and 600-grit paper, among others. The initial grit size is determined based on the sectioning depth and surface roughness, with 220 or 400 grit usually used after wire cut EDM sectioning. The last step in producing a flat, scratch-free surface is polishing. After grinding to a 2500-grit finish, the specimen should be polished further to eliminate all visible grinding scratches. To hold the abrasives in place during polishing, a polishing cloth is placed over a polishing wheel, and it is critical to ensure that there are no foreign objects on the polishing cloths that could damage the specimen's surface. Coarse polishing is frequently done with canvas, nylon, or silk, as they have little to no nap. Fine polishing, on the other hand, requires medium- or high-nap cloths, such as those made of densely packed synthetic fibers. When hand polishing with a polishing wheel, it is critical not to exert too much pressure on the specimen against the wheel as this could cause plastic deformation in the polished surface's top layer.

After cloth polishing, the samples should keep in the ultrasonic cleaner for 15 mins in a beaker with required amount of acetone to remove the layers from the sample.

For EBSD samples colloidal silica is used for polishing. Polishing is done for 1 hr for as-cast samples and for extruded samples the duration is 2-2.5 hrs. And master polish solution is prepared for this polishing step.

4.8.3 Etching

Etching is a technique used to make microstructural details on specimen surfaces more visible. It involves an electrolytic reaction between surfaces with various electrochemical potentials, which results in a controlled corrosion process. Due to differences in electrochemical potential during the etching process, chemicals called etchants selectively dissolve particular portions of the specimen surface, resulting in contrast between microstructural features.

Chapter 5

Results and Discussion

To investigate the microstructure, evaluate the microhardness, and conduct X-ray diffraction (XRD) analysis, 1 cm x 1 cm samples were cut from the core of each squeeze cast rod. For the purpose of analysing the microstructure, the cut specimens were polished and etched with 2% Nital (2% HNO3 + 98% ethanol), held for 3–4 seconds, and then optically investigated with an optical microscope (Zeiss AxioVert A1 inverted microscope). Phase analysis was performed using the XRD (Panalytical Empyrean and X'Pert High score). The microstructure and morphology of the phases were examined using a Field Emission Scanning Electron Microscope (FESEM, JEOL, JSM-7610 F plus) outfitted with an Energy Dispersive Spectrometer (EDS) and an Electron Backscatter Diffraction (EBSD). The phase compositions were quantitatively analysed using EDS. It was feasible to calculate the secondary dendrite arm spacing (SDAS) and estimated volume percentages of second phases present in the squeeze cast alloys in six different locations on the test samples using ImageJ software. The method for measuring SDAS is shown in Fig. 5.1 (an optical picture of the AZ91-Ca alloy was utilised). The number of cells was determined by dividing the measured length of the straight line that was created at the intersection of a group of cells that were all arranged in a row. The average grain size (AGS) of the sample was calculated using the EBSD method.

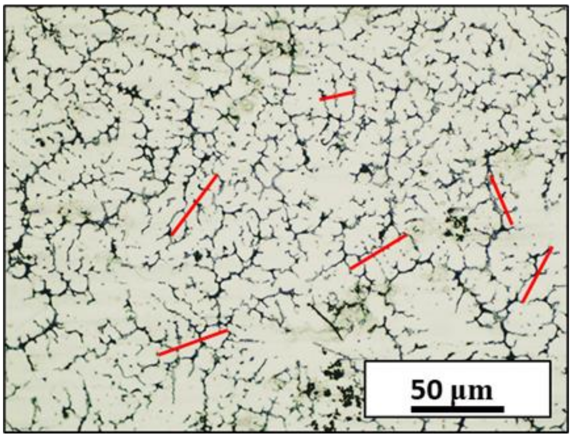

Fig.5.1: Measurement of SDAS shown in an optical micrograph of the AZ91-1 wt.% Ca alloy

5.1 Effect of Ca and Sr additions to as-cast AZ91 alloy

5.1.1 Phase analysis and microstructural characterization

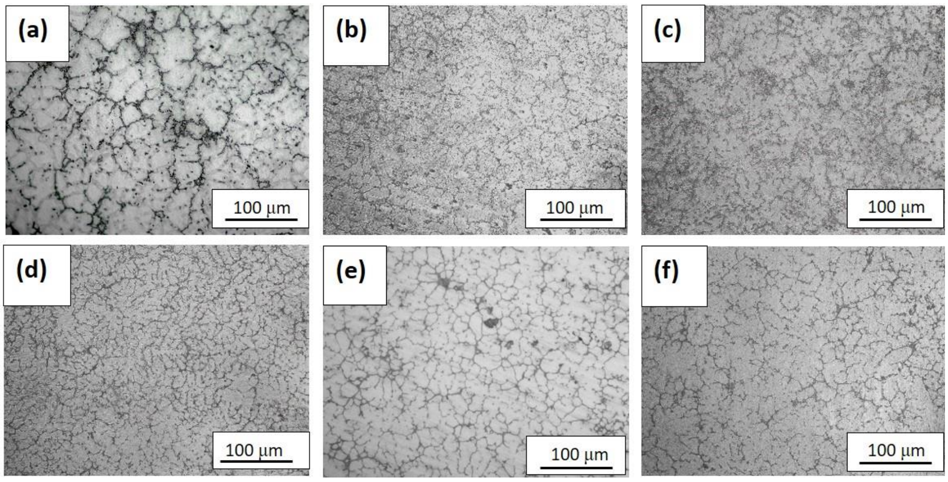

Fig.5.2: Optical micrographs of as-cast AZ91-Ca-Sr alloys (a)X1, (b)X2, (c)X3, (d)X4, (e)X5, (f)X6

Fig. 5.2 shows the optical micrographs of X1, X2, X3, X4, X5 and X6 alloy . The microstructure of AZ91 without addition (Fig.5.2 (a)) consists of α-Mg matrix and β-$Mg_{17}Al_{12}$ interdendritic network (β-phase). With Sr addition, the interdendritic network becomes continuous and refined (Fig. 5.2 (b)) and when addition of Sr increased from 0.3wt% to 0.6 wt.% the interdendritic network becomes more refine (Fig.5.2 (c)). Ca addition to base alloy AZ91 makes it finer and make some rosette like structure in the network (Fig.5.2 (d)). After Ca and Sr were added together, the novel

Al_2Ca and Al_4Sr lamellar phases developed (Fig. 5.2 (e)) and as the wt.% of Sr increases the Mg-Al-Sr phases also increases which makes the interdendritic network more finer and continuous (Fig. 5.2 (f)).

5.1.2 Secondary dendrite arm spacing measurement

The secondary dendrite arm spacing (SDAS) of the alloy X1, X2, X3, X4, X5 and X6 were compared. These numbers may provide information about how the inclusions of Ca and Sr impacted the rapid grain development. The secondary dendrite arm spacing (SDAS) of the interdendritic network is impacted by growth of the same with Ca and Sr addition. Fig. 5.3 illustrates the change in SDAS caused by Ca and Sr inclusions graphically. The findings show that adding Ca and Sr greatly reduces the SDAS, and that adding Ca refines the SDAS more than adding Sr does. The mechanical strength of the material is improved by the reduction in SDAS up to a certain point [6]; additionally, the reduction in grain size can be predicted by the drop in SDAS with Ca and Sr addition. In each alloy sample, the volume fractions of the Al_4Sr phases and total interdendritic network are plotted in Figure. An actual reduction in SDAS results from an increased number of nucleating sites [6].

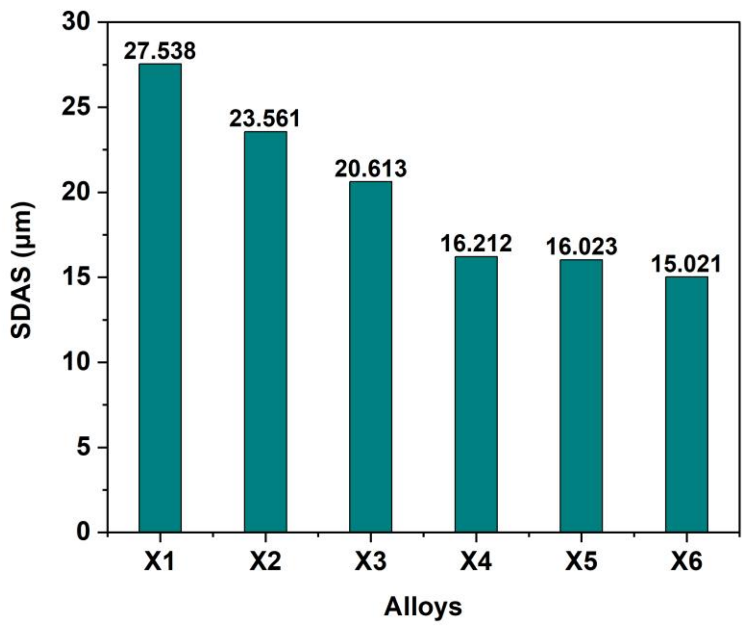

Fig.5.3: Calculated SDAS for squeeze cast AZ91 alloys

Fig.5.4 displays the XRD measurement data for each of the squeeze-cast alloys. The diffraction peaks and the Inorganic Crystal Structure Database (ICSD) are well matched. It's readily apparent from XRD graphs that each alloy is comprised of primary α-Mg and β-$Mg_{17}Al_{12}$ peaks. Due to their restricted solubility in the α-Mg, after addition of Ca and Sr to magnesium alloy causes Ca and Sr intermetallics development. These squeeze-cast alloys exhibit the presence of Al_2Ca and Al_4Sr phases in addition to these primary phases. The XRD measurement results for all the alloys show the presence of α-Mg and β-$Mg_{17}Al_{12}$, whereas the patterns show peaks for intermetallics like Al_2Ca and Al_4Sr for corresponding alloys. The peak intensity for the β -$Mg_{17}Al_{12}$ phase diminishes following the addition of Ca and Sr compared to the X1 alloy (base alloy AZ91) as shown in Fig. 5.4.

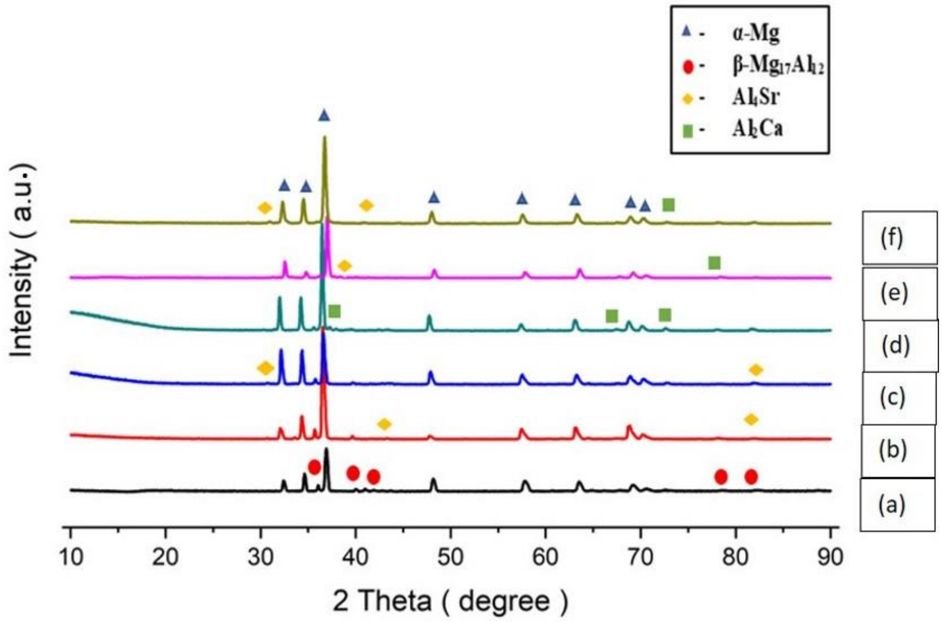

Fig.5.4: XRD analysis of squeeze-cast alloys

The suppression of β-$Mg_{17}Al_{12}$ with individual Ca and Sr addition has been studied in several literature studies [9, 17, 28]. L. Shang et al. [33] discovered β -$Mg_{17}Al_{12}$ phase is supressed by generating Al_2Ca, $Al_{11}Ce_3$, Al_4Sr, and Al_8CeMn_4 intermetallic phases using Ca, Sr, and Ce (0.2 wt% of each) as microalloying element in the AZ31.The author Y. Zhang et al.

[9] found that β-$Mg_{17}Al_{12}$ phase formation is quite entirely prevented with the 2 wt.% Ca addition in cast AZ91. With addition of 1wt.% Ca to cast AZ91D, the author Guohua Wu et al. [19] discovered a similar observation. Due to Ca and Sr's extremely low solubility in magnesium, which increases their availability for the production of second phases like Al_2Ca and Al_4Sr intermetallics, respectively, the volume fraction of β-$Mg_{17}Al_{12}$ has decreased. The suppression of β-$Mg_{17}Al_{12}$ is caused by aluminium atoms being devoured by Ca and Sr elements to generate Al_2Ca and Al_4Sr intermetallic compounds, which leaves less aluminium for interacting with the α-Mg matrix to make β-$Mg_{17}Al_{12}$.

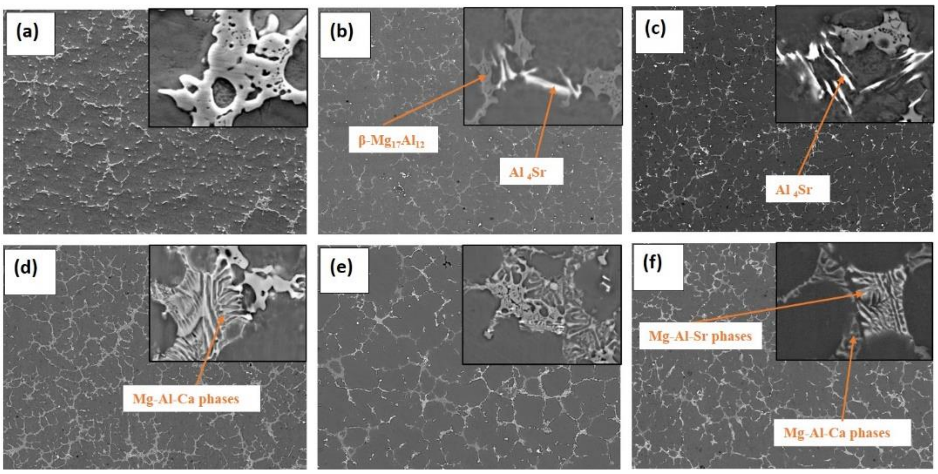

Fig. 5.5: FESEM micrographs of squeeze-cast alloys (a)X1, (b)X2, (c)X3, (d)X4, (e)X5 and (f)X6

The SEM microstructures of X1, X2, X3, X4, X5 and X6 alloys are shown in the Fig. 5.5. The main phases in X1 alloy is α-Mg matrix and β -$Mg_{17}Al_{12}$ (Fig. 5.5(a)). The addition of Sr to X1(base alloy AZ91), as shown in the figure, aids in the development of a continuous β-phase network and produces a bright pointed needle-like structure Al_4Sr intermetallics (Fig. 5.5(b)). As the Sr wt.% increases from 0.3 to 0.6, it creates more refined and continuous network. Moreover, the amount of needle-like Al_4Sr intermetallics also increases(Fig. 5.5(c)). With the addition of Ca, the bulk β -$Mg_{17}Al_{12}$ changed into the skeleton structure of Al_2Ca and $Mg_{17}Al_{12}$ mixed, which inhibited the formation of β -$Mg_{17}Al_{12}$ which is shown in Fig. 5.5(d). Following the addition of Ca and Sr, the novel Al_2Ca and Al_4Sr lamellar phases developed (Fig. 5.5(e),(f)), which have been confirmed by XRD analysis. Al_2Ca and β-$Mg_{17}Al_{12}$ appear to be a bit darker than the intermetallic Al_4Sr. With increased Sr addition, more continuous and refined phase network is produced (Fig. 5.5(e),(f)).

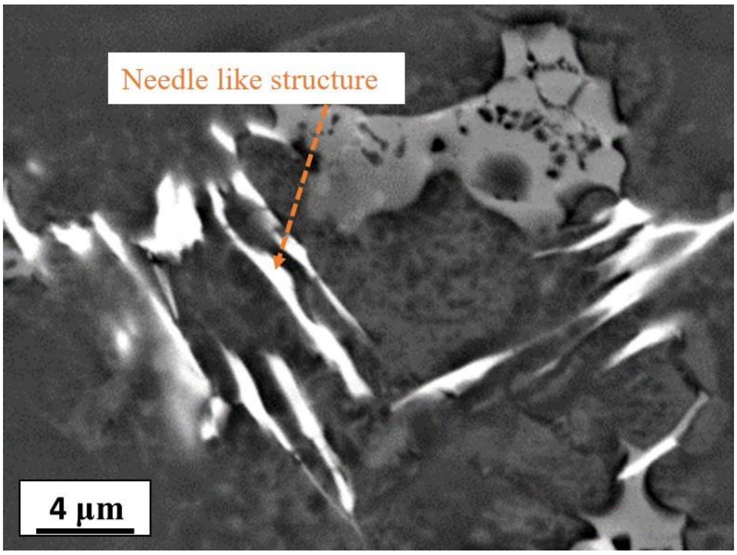

Fig.5.6: SEM micrograph of X3 alloy (AZ91-0.6wt.%Sr) showing needle-like structure

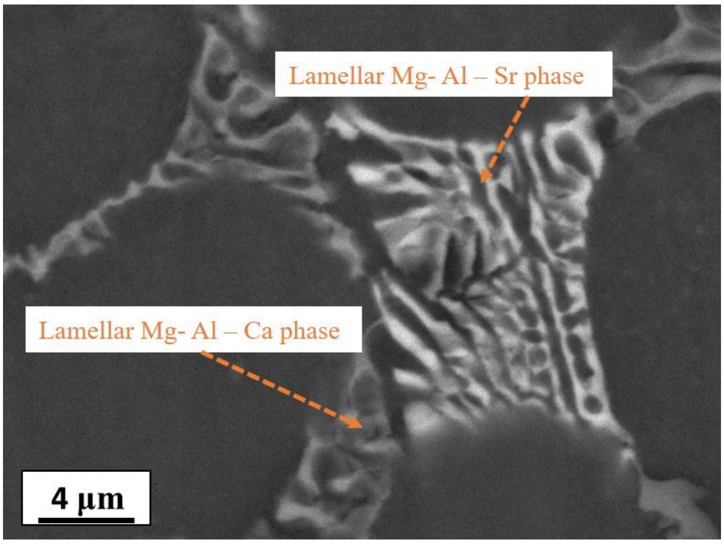

Fig.5.7: SEM micrograph of X6 alloy (AZ91- 1wt.%Ca-0.6wt.%Sr) showing lamellar Mg-Al-Ca-Sr phase morphology

With increasing Sr addition, it is discovered that the amount of lamellar network increases, which causes growing volume fraction of Al4Sr phases. Fig. 5.8 makes it clearly apparent that for alloys X2, X3, X5, and X6 with increase in weight percent of Sr addition, the volume fraction of the Al_4Sr

phase increases. Due to Al's higher affinity for Sr, the lamellar Al_4Sr network expands causing decrease in the β-phase. With an increase in Sr quantity, the interdendritic network's volume percentage has noticeably increased. The interdendritic network volume fraction in the X6 alloy was the highest due to the production of dense secondary phases. With increasing alloy addition, the interdendritic network's volume proportion of second phases rises.

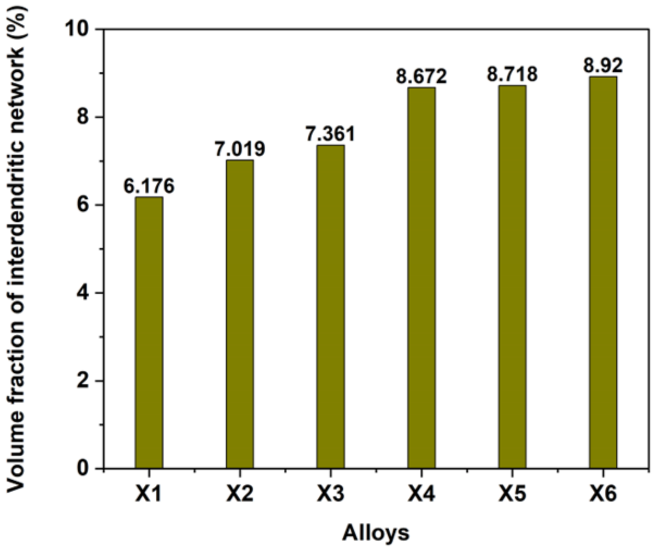

Fig.5.8: Volume fraction measurement of interdendritic network for all the alloys

Table 6: Values calculated for the interdendritic network volume fraction, the Al4Sr phase, and secondary dendrite arm spacing (SDAS) of squeeze - cast AZ91-Ca-Sr alloys

Alloys	Vol. fraction of interdendritic network (%)	Vol. fraction of Al4Sr phase (%)	SDAS (μm)
X1	6.176	-	27.538
X2	7.019	0.72	23.561
X3	7.361	1.815	20.613
X4	8.672	-	16.212
X5	8.718	1.22	16.023
X6	8.92	2.13	15.021

It is seen from the table 5 that the alloy X6 has the lowest value of SDAS and the highest volume fraction of interdendritic network as well as Al_4Sr phases. As a result of the development of dense secondary phase, the X6 alloy encountered the largest volume fraction of the interdendritic network (8.92 %).

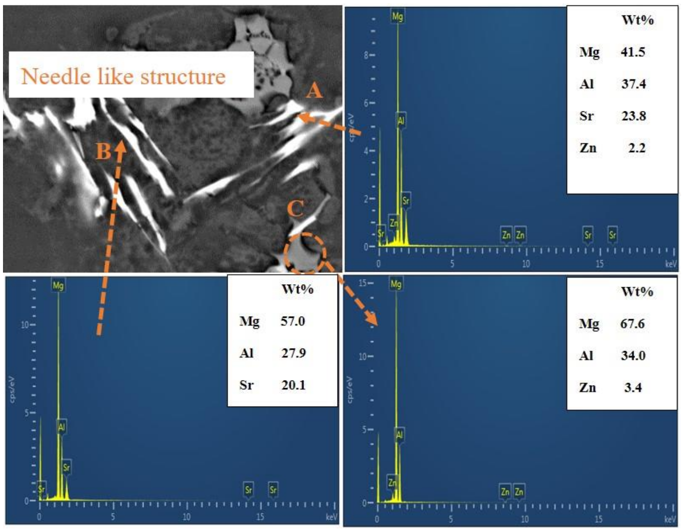

Fig. 5.9: BSE image of X3 alloy (AZ91- 0.6 wt.% Sr) with EDS spectrum of marked points.

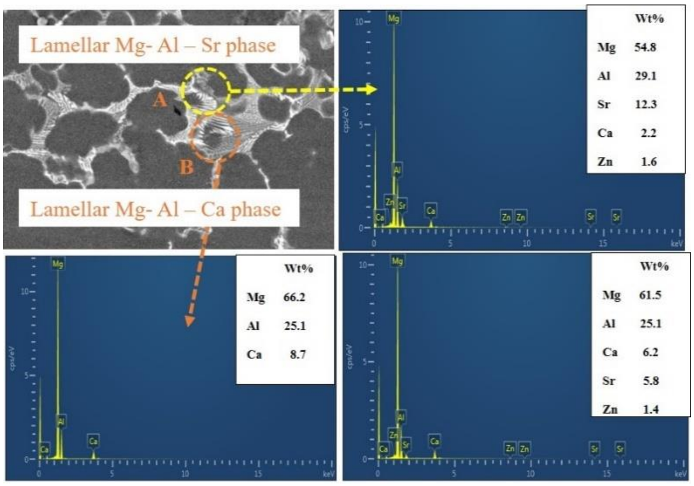

Fig. 5.10: BSE image of X6 alloy (AZ91-1 wt.% Ca - 0.6 wt.% Sr) with EDS spectrum of marked points

The Backscattered electron images and the corresponding EDS point analyses for the AZ91-Sr and AZ91- Ca-Sr alloy are shown in Figure 4.9 to analyse the morphology of all the phases and intermetallics present in the interdendritic network. The BSE image of X3 alloy (AZ91-0.6 wt% Sr) is shown in Figure 5.9. Al_4Sr intermetallics are seen in observations based on the weight percentage of the components in spectra A and B, while $Mg_{17}Al_{12}$ precipitates are seen in spectra C. It is clearly apparent from this EDS point analysis that the needle-like structure is primarily made up of Mg, Al, and Sr. On the BSE picture (Fig. 5.10), growing precipitates of Al_2Ca and a few Al_4Sr over the β-$Mg_{17}Al_{12}$ can be seen replacing bulky β-phase. In the BSE image of the X6 alloy (AZ91 -1 wt% Ca - 0.6 wt% Sr), Al_2Ca and Al_4Sr precipitates have completely developed lamellar structures (Figure 5.10). While spectrum B indicates bright Al_4Sr intermetallics, spectrum A displays a less-bright Mg-Al-Ca structure.

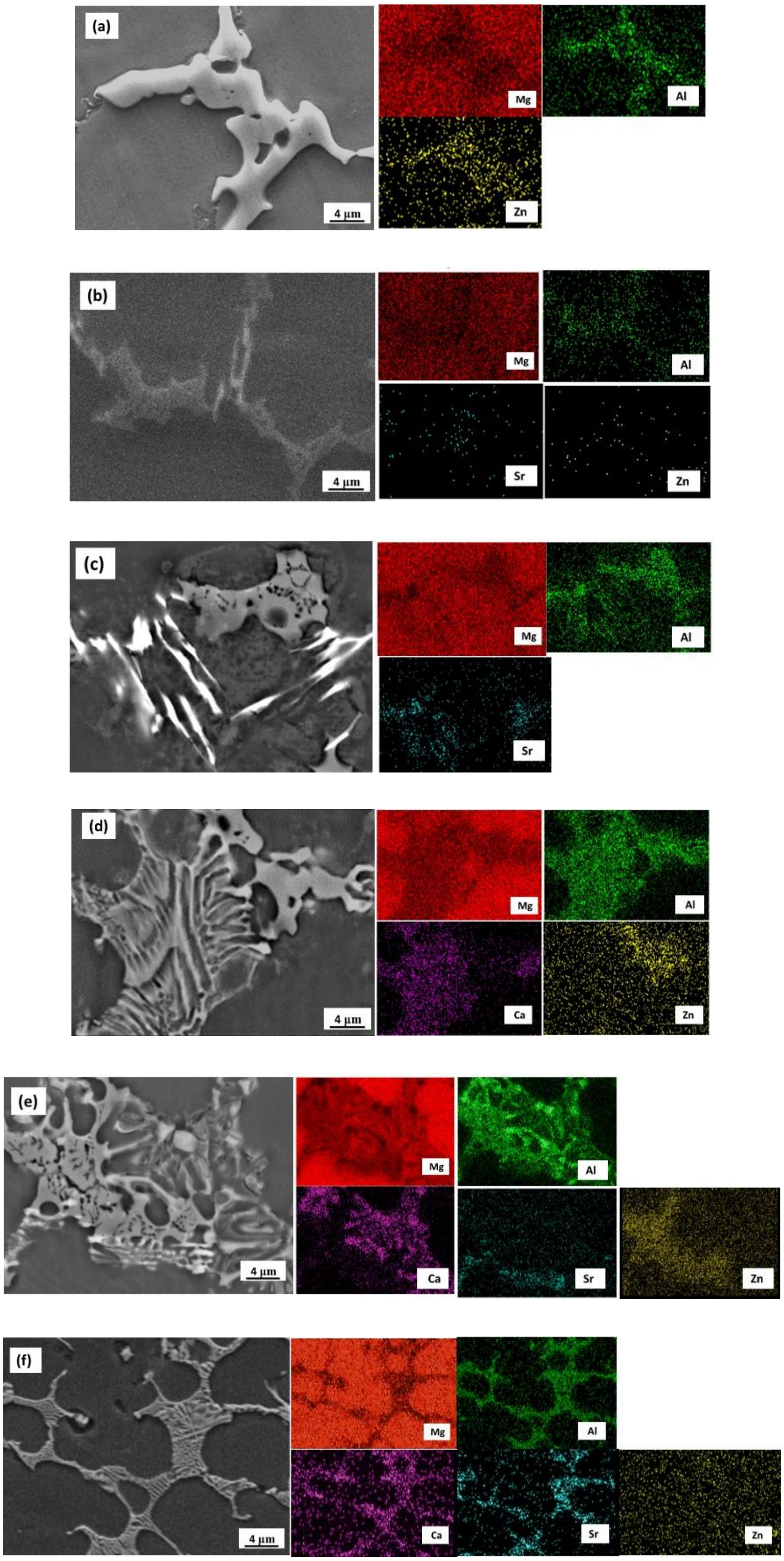

Fig.5.11: EDS color maps taken for all the squeeze cast alloys

The EDS mapping was done for the X1, X2, X3, X4, X5 and X6 samples as shown in Fig. 5.11, which shows the dispersion of various intermetallics and the associated elements. This was done to ensure the distribution of the Al_2Ca and Al_4Sr phase. The development of both Al_2Ca and Al_4Sr intermetallics is explained by the observation that the all intermetallics primarily comprise Al and also show the presence of Ca and Sr in their respective color maps . With a Ca content of 1 weight percent, the majority of the Ca dissolved in β-$Mg_{17}Al_{12}$ promotes the formation of the Al_2Ca phase and is dispersed at grain boundaries. The alloy X6 (Fig. 5.11(f)) with the maximum Sr content of 0.6% (keeping 1 wt.%Ca constant) exhibits the highest Sr rich regions in the interdendritic network in the respective EDS mapping, as expected. Additionally, the matrix sections have only a little amount of Ca and Sr content levels, indicating that the alloys X2 and X5 have Ca and Sr that are much less soluble in the matrix (α-Mg). Increasing the concentrations of Al-Ca and Al-Sr suppresses the production of the Al-Mg phase because all detected intermetallics are Al-based. The results of the EDS study agree with those of the prior FESEM observations.

5.1.3 Grain refinement of Squeeze cast alloys:

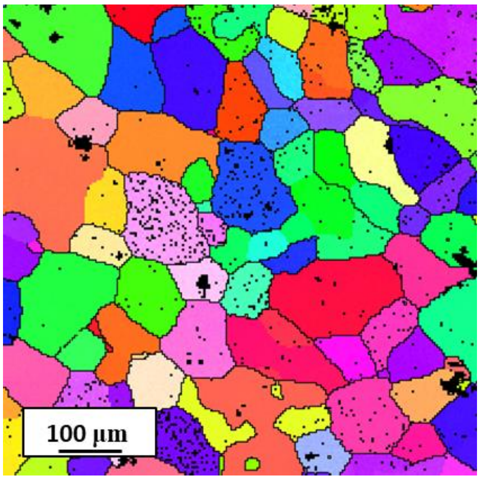

Fig.5.12: IPF map of X1 alloy

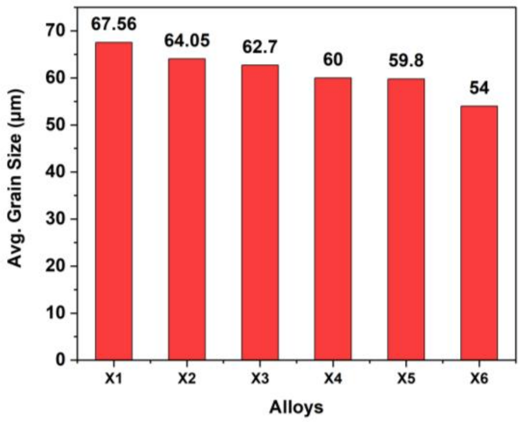

Fig.5.13: Avg. grain size of all six alloys

EBSD analysis was implemented to determine the average grain size of all the squeeze cast alloys. The IPF map of X1 alloy is shown in the Fig. 5.12 for reference. Fig. 5.13 shows the calculated average grain size of the alloys in the form of histogram plot. X1, X2, X3, X4, X5 and X6 have average grain sizes that are measured as 67.56 µm, 64.05 µm , 62.70 µm,60 µm, 59.8 µm and 54 µm respectively. It is clear that AZ91 has been refined through the addition of Ca and Sr.

5.1.4 Microhardness analysis

The average HV for each sample was plotted after the hardness was tested at 300 g load and 20 s dwell time. Fig. 4.14 provides a schematic representation of the regions where the hardness of the resulting squeeze cast rods was measured. For each sample, 6-8 readings were taken for calculating avg. microhardness value. The average microhardness values for all the samples are listed in the table 7.

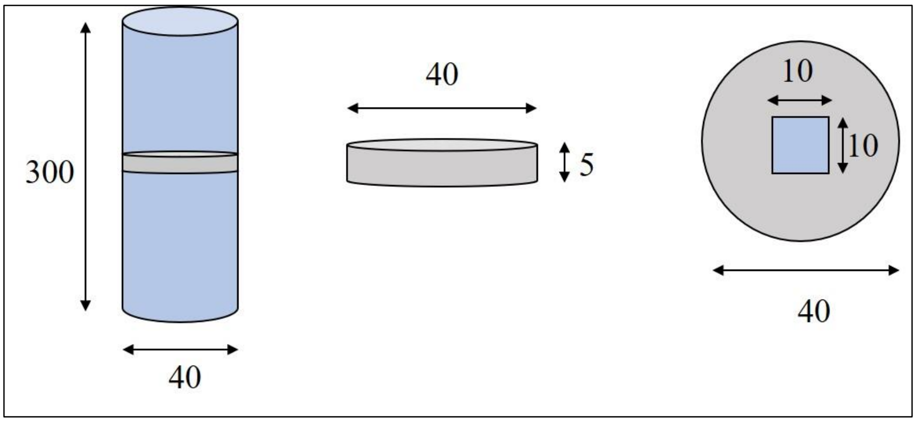

Fig.5.14: Sample dimension and region for the microhardness test (all the dimensions are in mm)

Table 7: Average microhardness value of X1-X6 alloys

Alloys	Hardness Value (HV)
X1	72.77 ± 2.90
X2	71.98 ± 2.62
X3	73.25 ± 1.80
X4	75.06 ±1.90
X5	74.12 ±2.71
X6	78.56 ±1.86

Vickers microhardness (HV) values for alloys X1 through X6 are illustrated in Figure 5.15 and listed in Table 7; these results show an upward trend in hardness values after alloy additions. Squeeze cast AZ91 alloy has an average Vicker's hardness rating of 72.77 HV. Fig. 4.15 shows that following preliminary Sr addition to AZ91, the hardness value somewhat decreases from X1 (72.77HV) to X2 (71.98 HV). After that, it is discovered that increasing the Sr addition from 0.3% to 0.6% causes hardness to rise from X2 (71.98 HV) to X3 (73.25HV). The hardness value of X1 alloy increase from 72.77 HV to 75.06 HV after the addition of 1wt.%Ca (only). There is slight reduction in hardness value after the addition of both Ca (1wt.%) and Sr (0.3wt.%) to the base alloy X1 and the hardness value of alloy X5 is 74.18. With the addition of 1wt.%Ca and 0.6wt.%Sr, the alloy X6 has the highest hardness value which is 78.56 HV.

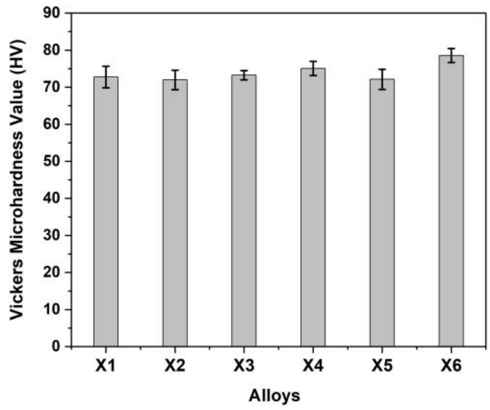

Fig. 5.15: Vickers microhardness value for all the alloys

5.1.5 Tensile properties:

For all of the alloy samples used in the current research, the values of TYS, UTS, and% elongation evaluated using tensile testing are plotted in the figure. Fig. 4.16 shows various tensile property variation with composition alteration for the samples X1, X3, X4 and X6.

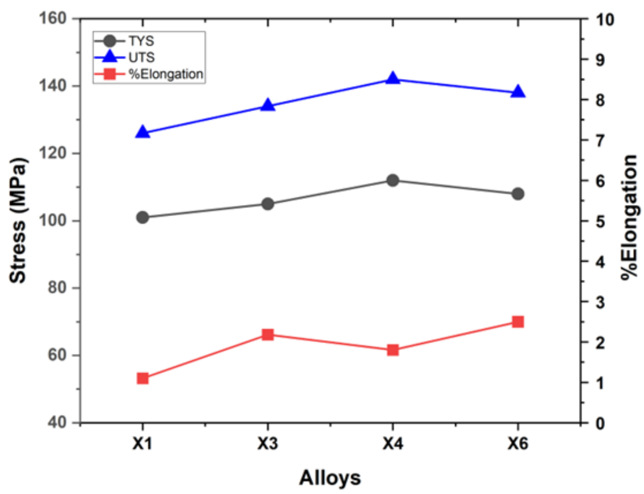

Fig.5.16: Effect of Ca and Sr on mechanical properties of squeeze cast AZ91 alloys in tensile (TYS – tensile yield stress, UTS – ultimate tensile stress)

It is observed that, addition of 0.6wt.%Sr (alloy X2) has improved the TYS and UTS compared to base AZ91alloy. The TYS and UTS has lower value at 1wt.%Ca+0.6wt.% Sr (alloy X6) addition than only 1wt.%Ca (alloy X4) addition whereas highest elongation obtained at the same.

5.2 Extruded AZ91 alloys

5.2.1 Extruded microstructures study

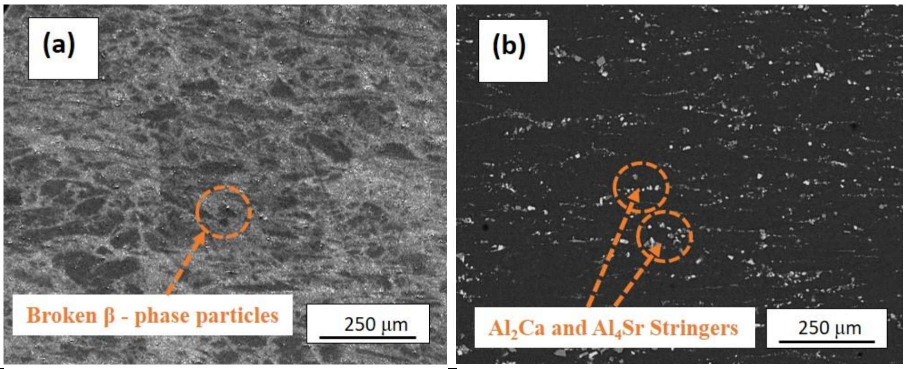

Fig.5.17: SEM micrographs of extruded alloys (a) AZ91 (b) AZ91 - 1wt%Ca-0.6wt%Sr (along extruded direction)

After the extrusion process the large beta particle breaks down into small particle which is shown in Fig.5.17 (a). Post extrusion deformation, the second phase displays a stringer distribution along the extrusion direction. In the microstructure, second-phase particles develop as a result of the addition of Ca and Sr. The mechanical properties of the alloy can be influenced by these particles, which can act as nucleation sites for the refining of the magnesium grains. These particles can show up inside the matrix as tiny, scattered particles. Based on the findings, the second phase was continuously crushed and deformed before taking on a granular morphology. However, the majority of the β-$Mg_{17}Al_{12}$ phase, Al_2Ca, and Al_4Sr phases are dispersed along the extrusion direction in the longitudinal section of the extruded Mg alloy, and a small number of them are distributed independently on the matrix. The Al_4Sr and Al_2Ca intermetallics are broken down into smaller particles during the extrusion process and distributed along the extrusion direction as depicted in Fig. 5.17 (b) for the alloy AZ91-1wt.%Ca-0.6wt.%Sr. In comparison to the cast, these broken and minute particles can reduce the number of possible sites for the start and spread of cracks during tensile tests.

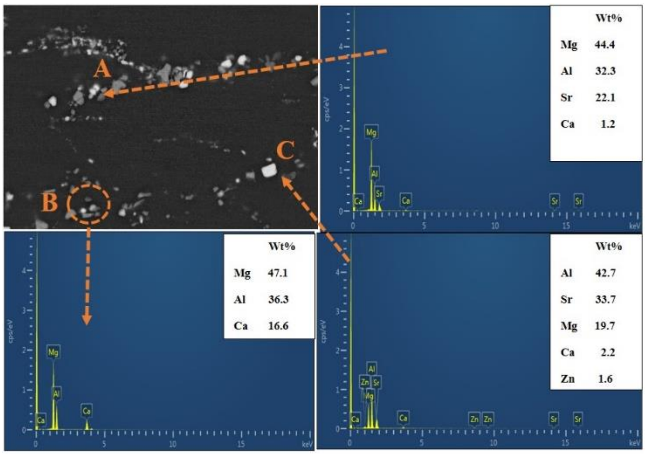

Fig.5.18: EDS point analysis of AZ91-1wt.%Ca-1wt.%Sr extruded alloy

To study the phase morphology of all the intermetallics and phases present in the AZ91-1Ca-0.6Sr alloy, the BSE pictures and accompanying EDS point analysis are displayed in Fig. 5.18. Observations based on the weight % of the constituents in spectra A and C show the presence of Al_2Ca and Al_4Sr broken elongated intermetallics, whereas spectra B only show Al_2Ca precipitates. This EDS point analysis makes it very clear that the main components of the stringers structure are Mg, Al, Sr, and Ca.

5.2.2 Stringer formation

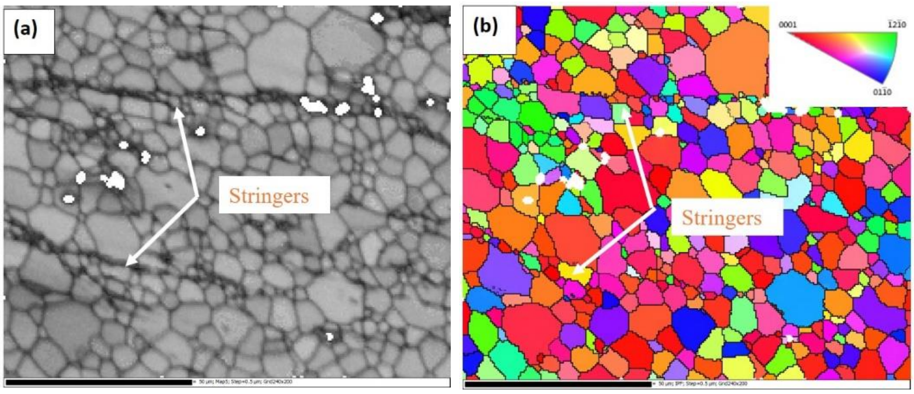

Fig.5.19: EBSD microstructure of extruded AZ91-1wt.%Ca-0.6wt.%Sr alloy (a) IQ map (b) Orientation map

The EBSD orientation map of AZ91-1wt.%Ca-0.6wt.%Sr alloy extruded at 400 °C is shown in Fig. 5.19(b). Elongated parent grains and small and big recrystallized grains constitute the microstructure. The colors of the grains' represent their distinct orientations. Parent grains that are elongated exhibit progressive colour variations that signify local deformation and low-angle grain boundaries. It should be noted that recrystallized grains can be found both near and far from intermetallic stringers.

5.2.3 XRD texture analysis

It was observed that after the addition of Ca and Sr to AZ91 alloy, the intensity of the basal textures are reduced. That means the addition of Ca and Sr weakens the texture of the alloy which helps in improving the mechanical properties (which will be discussed in upcoming section). This texture analysis was done with the help of XRD in the direction which is perpendicular the extruded direction of the sample.

5.2.4 Grain size measurement

Grain size distribution plot for both the extruded alloys are shown the following Fig.5.20. The calculated average grain size diameter for AZ91 extruded alloy is 8.52 μm and for AZ91-1wt.%Ca-0.6%Sr the value is 6.14 μm. This means, after the combined addition of Ca and Sr there is reduction in grain size diameter, Ca and Sr refines the grains. The percentage reduction in grain size after the addition of Ca and Sr is 27.93%.

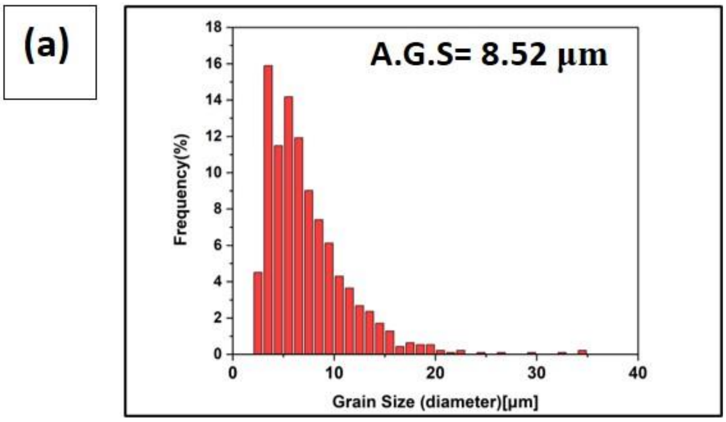

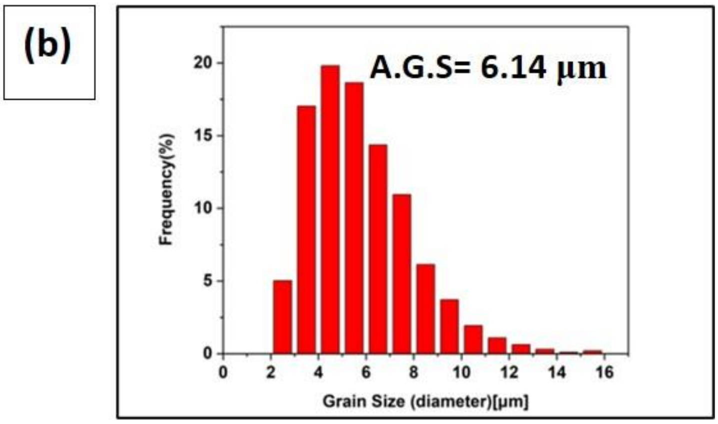

Fig.5.20: Grain size distribution of extruded alloys (a)AZ91, (b)AZ91-1wt.%Ca-0.6wt.%Sr

5.2.5 Recrystallisation

Unrecrystallized and recrystallized grains that have undergone deformation are the characteristics of the microstructure. Al_2Ca and Al_4Sr stringers that have been found in the as-cast microstructure are extended in the direction of extrusion as it has been seen in SEM micrographs. In the microstructure, there are two different types of recrystallized grains that are observed to form both around the stringers and at the grain boundaries of undeformed grains. In the microstructure, intermetallic stringers are dispersed, and recrystallization is observed both in the matrix and surrounding the stringers.

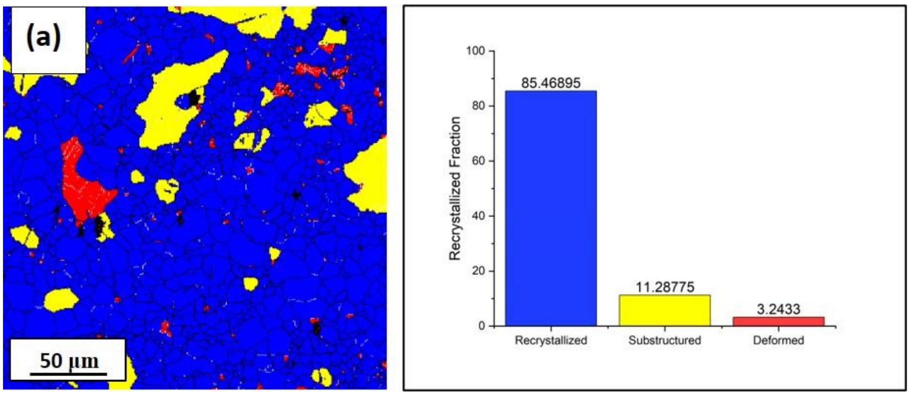

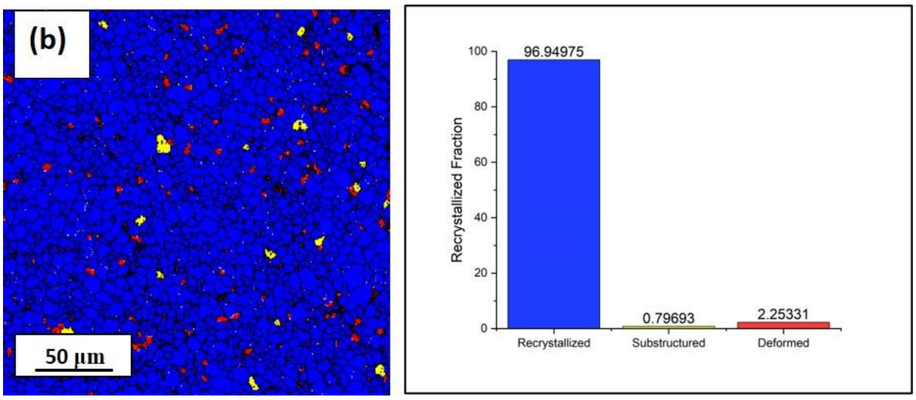

Fig.5.21: Recrystallized fraction of extruded alloy (a) AZ91 and (b)AZ91-1wt.%Ca-0.6wt.%Sr

Fig. 5.21 shows that after the alloy addition the recrystallized fraction increased from 85.47% to 96.95%. And the fraction for substructured grains reduces from 11.29% to 0.79% for the AZ91-1wt.%Ca-0.6wt.%Sr alloy.

5.2.6 Mechanical Properties

Tensile yield stress rises with the addition of Ca and Sr, although ultimate tensile stress increases relatively less (Table 8). Due to the reduction in grain size, the additions of Ca and Sr still exhibit higher values of elongation than the base alloy AZ91(Table 8). The yield asymmetry of AZ91 alloy was found to be reduced by the addition of Ca and Sr. CYS/TYS values grow from 0.78 (AZ91) to 0.82 (AZ91-1wt.%Ca-0.6wt.%Sr) which is listed in Table 10. Lowering yield asymmetry in magnesium alloys can significantly increase their formability because it will improve their ability to perform in applications that require bending for example.

Table 8: Tensile test performed for extruded alloys

Alloys	**TYS (MPa)**	**UTS (MPa)**	**%Elongation**
AZ91	278	365	9
AZ91-1wt.%Ca-0.6wt.%Sr	289	371	4.8

Table 9: Compression test performed for extruded alloys

Alloys	**CYS (MPa)**	**UCS (MPa)**	**%Elongation**
AZ91	218	523	15.2
AZ91-1wt.%Ca-0.6wt.%Sr	237	485	13

Table 10: Calculated CYS/TYS ratio

Alloys	**CYS/TYS**
AZ91	0.78
AZ91-1wt.%Ca-0.6wt.%Sr	0.82

The grain size and texture have a significant impact on the mechanical properties of extrusions. As Ca and Sr are added, the grain size of the AZ91 alloy reduces. Due to its large grain size, the AZ91 alloy also exhibits the lower TYS value. The basal texture that is generated in AZ91 will promote compression loading along the extrusion direction rather than tensile loading. With CYS/TYS = 0.78, AZ91 exhibits the maximum yield asymmetry. Ca and Sr additions randomise the texture and reduce the grain size of AZ91, which reduces the yield asymmetry.

5.3 Microstructure and Microhardness of Squeeze-cast AZ91 Mg Alloy with Ca, Sr and Ce Additions

5.3.1 Microstructural study of as-cast alloy

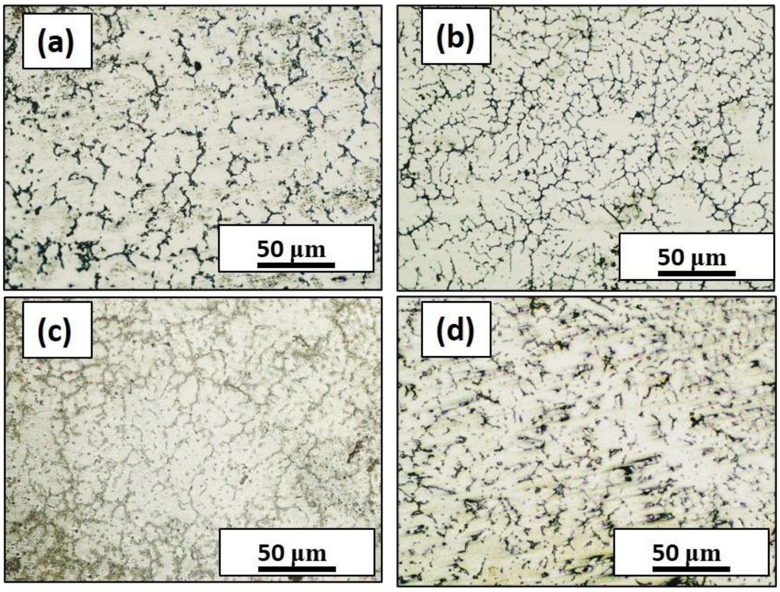

Fig.5.22: Optical micrographs of the squeezing cast alloys showing dendritic microstructure (a) AZ91 (b) AZ91 - 1wt.% Ca (c) AZ91-1wt.% Sr (d)AZ91-1wt.%Ce alloys

The optical micrographs of the alloys AZ91, AZ91-1wt.% Ca, AZ91-1wt.% Sr, and AZ91-1wt.% Ce are shown in Fig.5.22. The interdendritic network of β-$Mg_{17}Al_{12}$ and the α-Mg matrix make up the microstructure of AZ91 without any alloying element (Fig. 5.22(a)). The interdendritic network becomes more continuous and refined with the addition of Ca and Sr separately (Fig. 5.22(b), (c)), but the β-phase displays a discontinuous network with the addition of Ce (Fig. 5.22(d)).

The secondary dendrite arm spacing (SDAS) of AZ91, AZ91-1wt.% Ca, AZ91-1wt.% Sr, and AZ91-1wt.% Ce were compared. The cast alloys' predicted SDAS are 27.538 m, 16.212 m, 16.918 m, and 17.979 m, respectively, for the alloys AZ91, AZ91- 1wt.% Ca, AZ91-1wt.% Sr, and AZ91- 1wt.% Ce. These data might be used to determine how the additions of Ca, Sr, and Ce affected the fast growth of the grain. Fig.5.23 depicts the change in SDAS caused by the addition of Ca, Sr, and Ce graphically. The findings show that the SDAS greatly declines with the addition of Ca, Sr, and Ce, and that the addition of Ca refines the SDAS more than Sr and Ce do. Following the addition of Ca, Sr, and Ce, Fig.5.24 shows the estimated volume percentage of the interdendritic network of the alloys β-phase Contrary to Sr and Ce addition, it has been found that Ca addition produces a greater volume proportion of the interdendritic network.

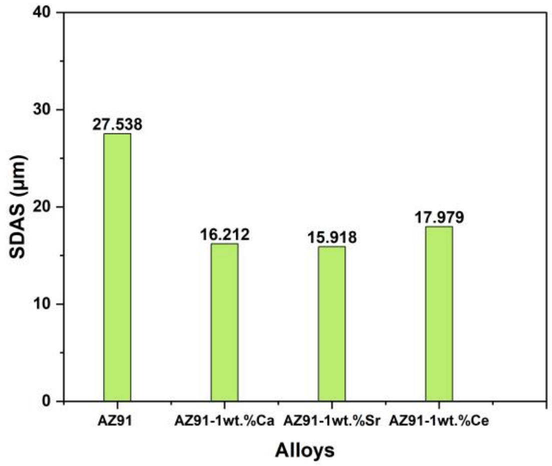

Fig.5.23: SDAS values plotted for all the alloys

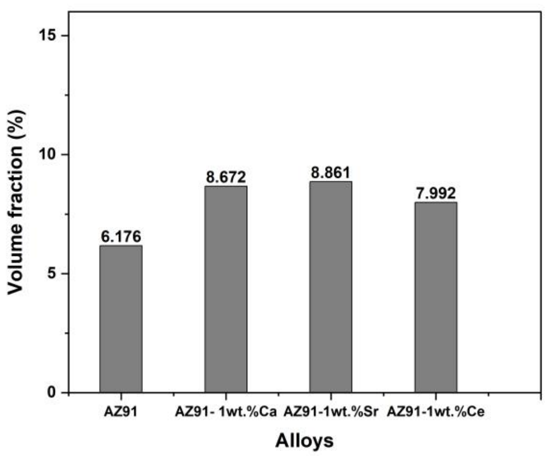

Fig.5.24: Volume fraction of interdendritic network plotted for all the alloys

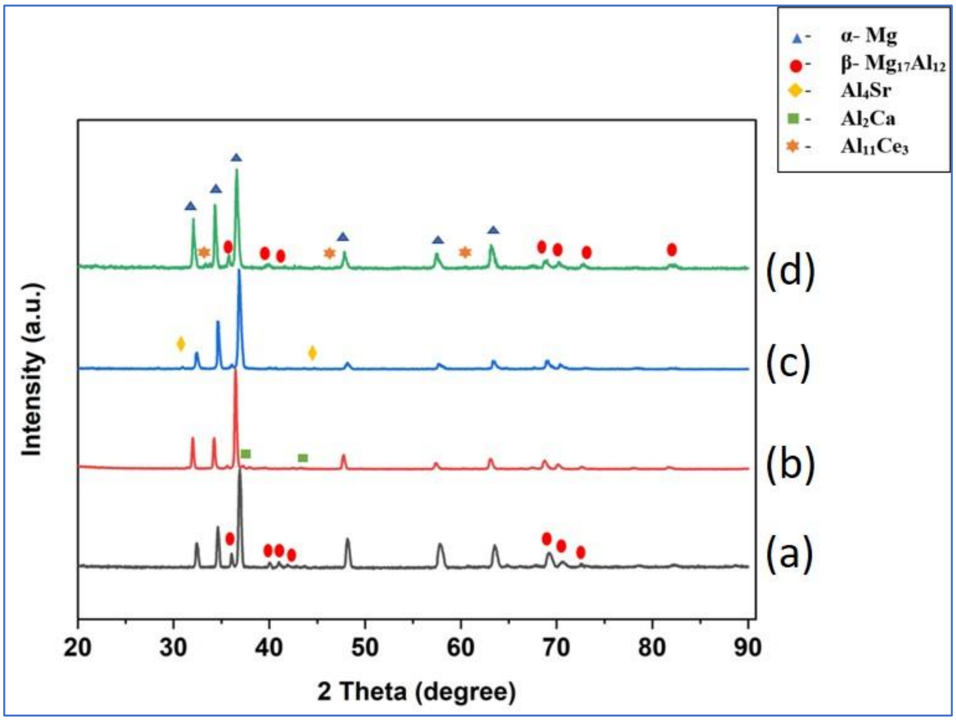

Fig.5.25: XRD analysis of all the cast samples(a) AZ91 (b) AZ91 - 1wt.% Ca (c) AZ91-1wt.% Sr (d)AZ91-1wt.%Ce

With the help of XRD analysis, Al_2Ca, Al_4Sr and $Al_{11}Ce_3$ peaks has been detected for the alloys (a) AZ91 (b) AZ91 - 1wt.% Ca (c) AZ91-1wt.% Sr (d)AZ91-1wt.%Ce, respectively Fig. 5.25.

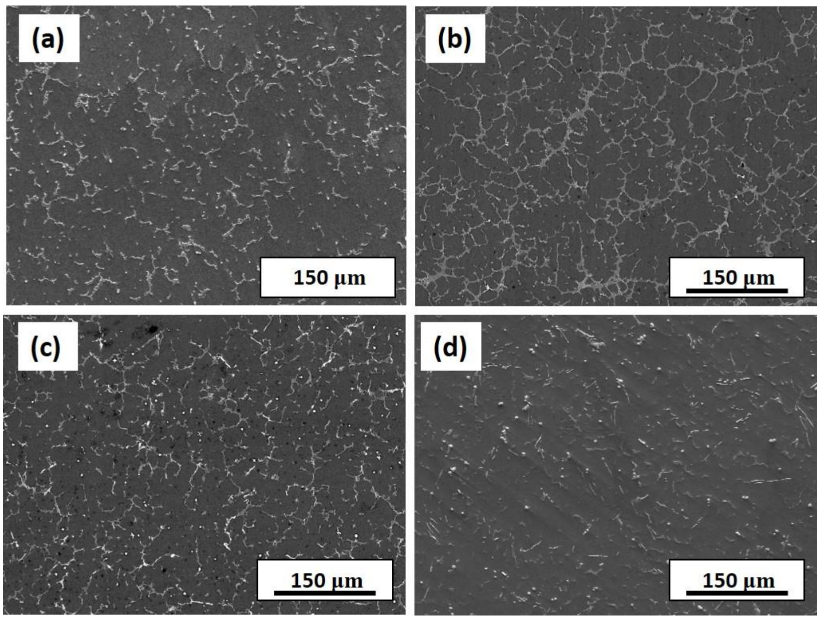

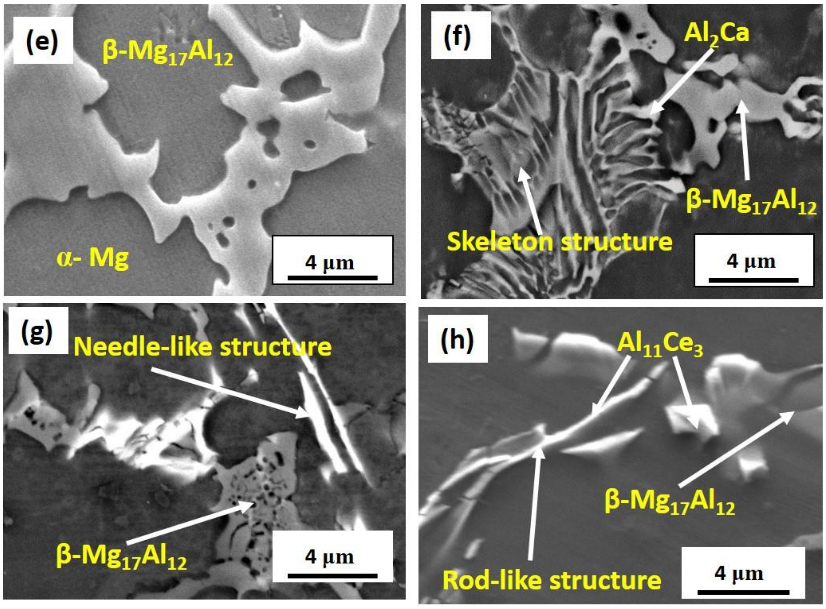

Fig.5.26: SEM micrographs of (a) AZ91 (b) AZ91 - 1wt.% Ca (c) AZ91-1wt.% Sr (d)AZ91-1wt.%Ce alloys and magnified SEM micrographs of (e) AZ91 (f) AZ91 - 1wt.% Ca (g) AZ91-1wt.% Sr (h)AZ91-1wt.%Ce alloys showing phase morphologies

The FESEM micrographs of the alloys AZ91, AZ91 - 1wt% Ca, AZ91 - 1wt% Sr, and AZ91 - 1wt% Ce are shown in Figure. According to Fig. 5.26(a), the major components of AZ91 alloy are α-Mg and β-$Mg_{17}Al_{12}$. Ca and Sr addition to the base alloy AZ91 both contribute to the development of a continuous β -phase network, as seen in Fig. 5.26(b) and (c), respectively. When Ce is added to the AZ91 alloy, the β-phase is refined and forms a discontinuous interdendritic network, as seen in Fig. 5.26 (d). To better see the morphology of the phases, Figs. 5.26 (e), (f),(g), and (h) show magnified FESEM images of the AZ91, AZ91-1Ca, AZ91-Sr, and AZ91-Ce alloys, respectively. The microstructure of the bulk β-phase-containing AZ91 alloy is shown in Fig. 5.26(e). Following the addition of Ca, the bulk β-$Mg_{17}Al_{12}$ changed into the skeleton structure of mixed $Mg_{17}Al_{12}$ and Al_2Ca, which inhibited the formation of β-$Mg_{17}Al_{12}$ (Fig. 5.26(f)). After adding Sr to AZ91 alloy, Fig. 5.26 (g) depicts the development of a bright needle-like pointed structure of Al_4Sr intermetallics. $Al_{11}Ce_3$ phase, which has a rod-like structure, is formed in the AZ91 alloy once Ce is added. $Al_{11}Ce_3$ precipitates are evenly distributed throughout the alloy as thin rods (Fig. 5.26(d) and (h)), and they can be easily separated from β-$Mg_{17}Al_{12}$ precipitates by their light white colour as opposed to the latter's more typical grey appearance.

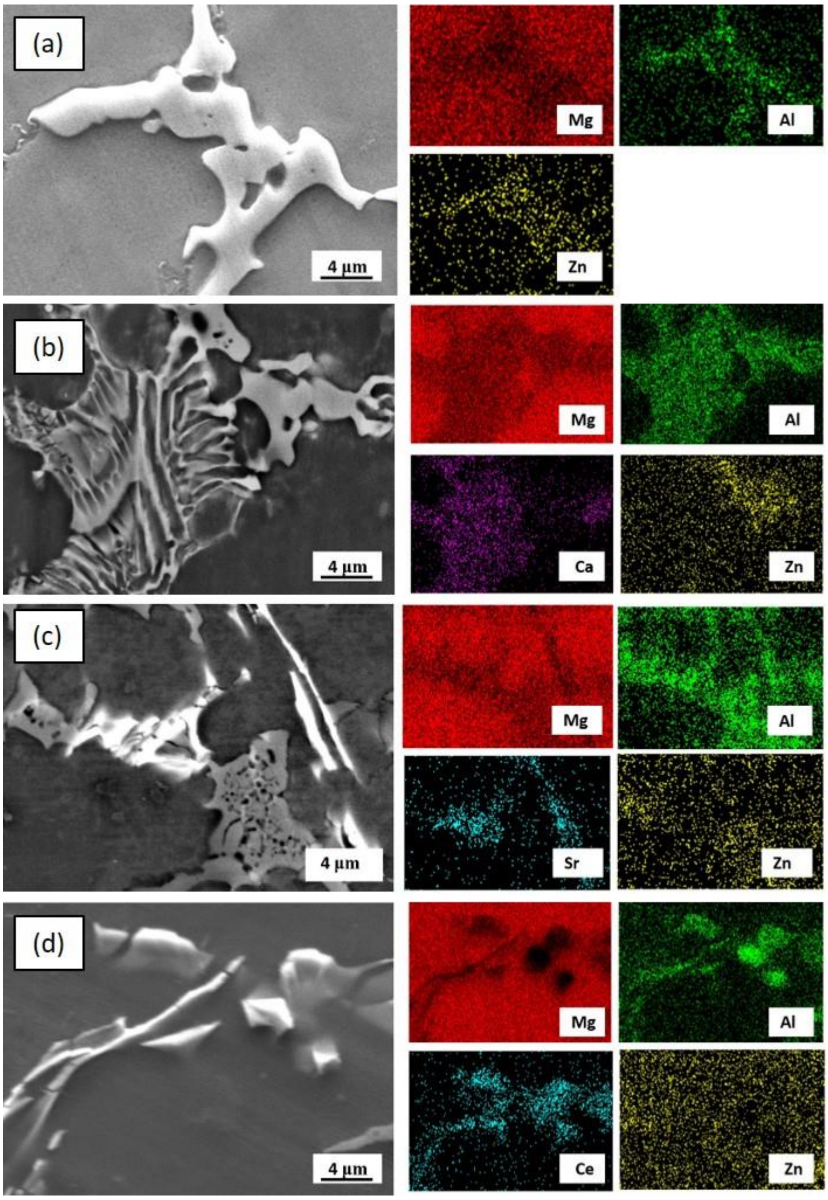

Fig.5.27: EDS color maps for the alloys (a) AZ91 (b) AZ91 - 1wt.% Ca (c) AZ91-1wt.% Sr (d)AZ91-1wt.%Ce

Fig. 5.27 illustrates the EDS mapping of all four alloys, which ensures the distribution of the phases β-$Mg_{17}Al_{12}$, Al_2Ca, Al_4Sr, and $Al_{11}Ce_3$. It also shows how it distributes of various intermetallics and their respective elements. The fact that all intermetallics largely consist of Al and also indicate the presence of Ca, Sr, and Ce in their respective maps (Figs.5.27 (b), (c), and (d)) helps to explain the evolution of intermetallics such as Al_2Ca, Al_4Sr, and $Al_{11}Ce_3$. Fig. 5.27 (b) demonstrates that Al_2Ca and the β-$Mg_{17}Al_{12}$ phase make up the majority of the skeleton structure formation in the AZ91-1wt% Ca alloy. The Al_4Sr needle-like structure in Fig. 5.27(c) is mostly made up of Al and Sr components. The development of $Al_{11}Ce_3$ intermetallics with a 1 wt.% Ce addition is implied by Fig. 5.27(d), which fully explains the existence of Al and Ce elements in the rod-like intermetallic phases.

5.3.2 Grain refinement in AZ91-1 wt.% Ca, AZ91-1wt.%Sr and AZ91-1 wt.% Ce alloy

EBSD analysis was used to establish the average grain size. The inverse pole figure (IPF) maps for all four alloys are shown in Fig. 5.28. In comparison to AZ91-Ca, AZ91-Sr, and AZ91-Ce, base alloy AZ91 is seen to have coarser grains in its microstructure. Fig. 5.29 in this section shows the measured average grain size and grain size distribution plot. AZ91, AZ91-1wt.% Ca, AZ91-1wt.%Sr, and AZ91-1wt.% Ce have average grain sizes that are measured at 69.16 μm, 52.05 μm, 41.31μm and 47.62μm respectively. It is clear that AZ91 has been refined through the inclusion of Ca, Sr, and Ce.

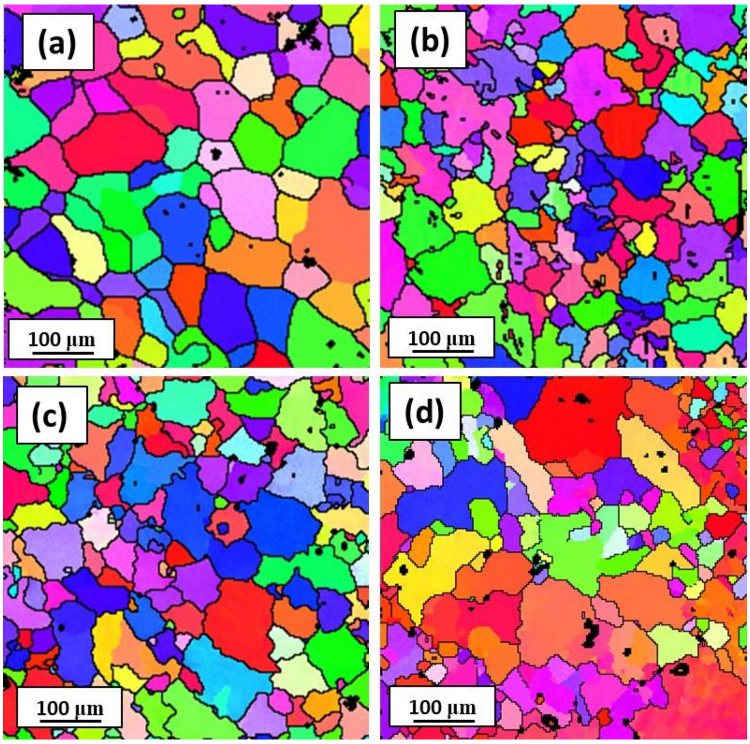

Fig.5.28: EBSD IPF maps of alloys (a) AZ91 (b) AZ91 - 1wt.% Ca (c) AZ91-1wt.% Sr (d)AZ91-1wt.%Ce

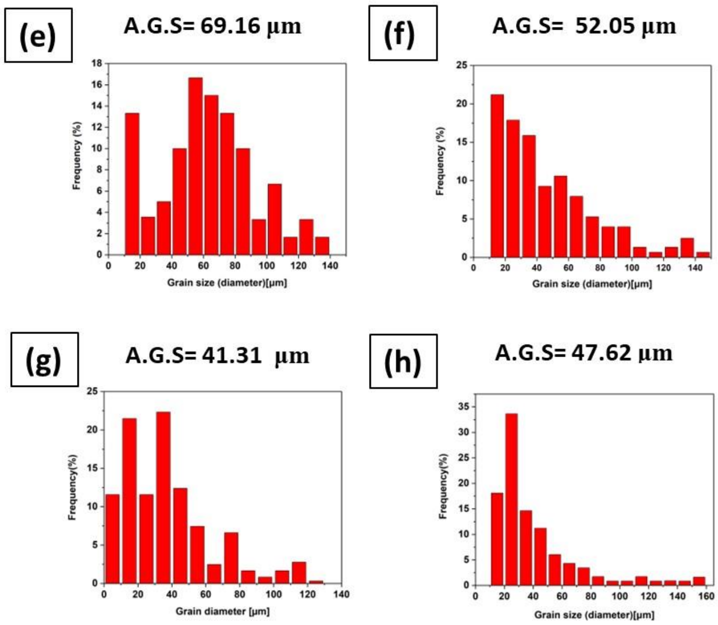

Fig. 5.29: Grain size distribution plot and AGS values of alloys (a) AZ91 (b) AZ91 - 1wt.% Ca (c) AZ91-1wt.% Sr (d)AZ91-1wt.%Ce

When Ca, Sr, and Ce are added to AZ91 alloy, the intermetallics creation produces heterogenous nucleation sites that allow for the production of new grains when the alloy solidifies. Additionally, intermetallics Al_2Ca, Al_4Sr, and $Al_{11}Ce_3$ are pinned at the grain borders and limit grain expansion. The addition of Ca, Sr, and Ce to the AZ91 alloy caused a grain refining effect that reduced AGS by 24.74%, 40.27% and 31.15%, respectively.

5.3.3 Microhardness analysis for all the squeeze-cast alloy

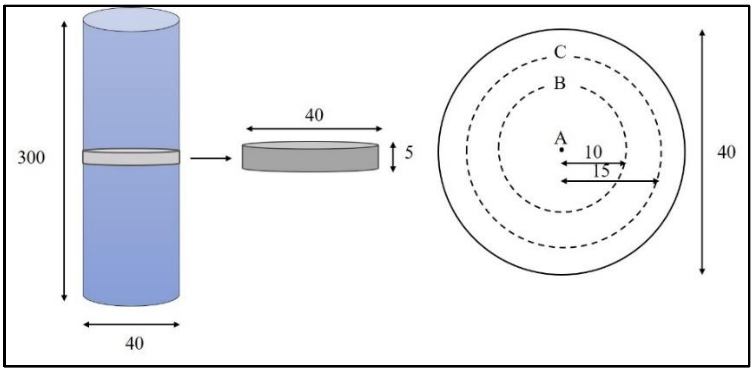

Fig. 5.30: Hardness test specimen with different zones (all the dimensions are in mm)

The values for Vickers microhardness are displayed in Fig. 5.31 and summarised in Table 11. In the test specimen for each alloy, the hardness values are computed in three separate zones (from the centre to the edge) Fig.5.30. For AZ91, the average hardness value for the central region is 72.77 HV (Fig. above , zone A), and the hardness value increases from the centre to the edge regions (74.06 HV for zone B and 78.92 HV for zone C, respectively). For AZ91-1wt.% Ca, AZ91-1wt.% Sr, and AZ91-1 wt.% Ce alloys, a similar tendency has been noted. For the alloys AZ91, AZ91-1wt.% Ca, AZ91-1wt.% Sr, and AZ91-1wt.% Ce, the percentage increase in hardness values from centre to edge is 8.45%, 6.75%, 8.29%, and 5.02%, respectively.

Table 11: Calculated Vickers microhardness values for cast alloy

Distance from the centre (mm)	Vickers microhardness values for alloys (HV)			
	AZ91	AZ91 – 1wt.% Ca	AZ91-1wt.%Sr	AZ91-1wt.%Ce
0	72.77 ± 2.9	75.06 ±1.9	73.01± 2.2	80.65 ±1.35
10	74.06 ±1.52	76.57 ±2.1	74.04± 1.89	81.75 ±1.62
15	78.12 ±2.7	80.13 ±1.3	79.06± 1.67	84.70 ±3.02

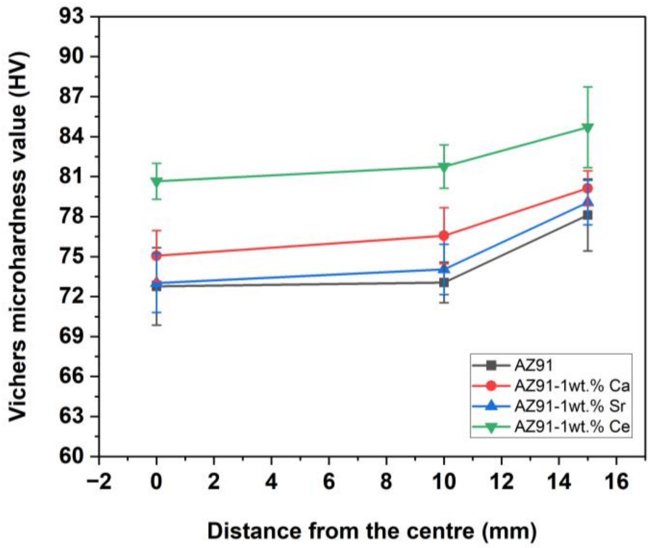

Fig.5.31: Vickers microhardness value plotted for all four samples

After alloying AZ91 with Ca, Sr, and Ce additions, the hardness values are observed to increase (Fig. 5.31). For AZ91-1wt.% Ca, AZ91-1wt.%Sr, and AZ91-1wt.% Ce, respectively, the percentage increase in average hardness value (considering the centre region) is 3.15%, 0.38%, and 10.83% when compared to basic AZ91 alloy. After the addition of Ca, Sr, and Ce, tougher intermetallics (Al_2Ca, Al_4Sr, and $Al_{11}Ce_3$) were created that were resistant to the indenter force and had higher hardness values. The improvement in hardness was also aided by the grain refinement that resulted from the addition of Ca, Sr and Ce to the alloy structure.

Chapter 6

Conclusion and Future Scope

In the current study, the impact of individual Ca and Sr additions as well as combined additions of Ca and Sr to squeeze-cast AZ91 alloy was investigated. Studying the microstructures of the alloys, testing their hardness and tensile properties and measuring the average grain size for all the squeeze-cast alloys were done.

6.1 Conclusions

AZ91-1Ca-0.6Sr has the optimal characteristics out of all these six squeeze-cast alloys. Therefore, the AZ91 alloy and AZ91-1Ca-0.6Sr is examined in the extruded section, including texture, microstructure analysis and mechanical properties. In this work, the individual effects of Ca, Sr, and Ce on the squeeze-cast AZ91 alloy are also investigated. The findings of the current investigation led to the following conclusions :

- Continuous and finer secondary phase interdendritic network was produced after Ca and Sr were added to AZ91. It becomes more continuous and refined when Ca and Sr are added together to the AZ91 alloy. After the addition of Ca and Sr to the AZ91 alloy, the drop in SDAS value was noticed.
- Al_4Sr intermetallics with a bright white needle-like structure are formed when Sr is added to the AZ91 alloy, suppressing the β-$Mg_{17}Al_{12}$ phase. After the addition of Ca, the bulk β-$Mg_{17}Al_{12}$ phase underwent transformation into the mixed Al_2Ca and $Mg_{17}Al_{12}$ skeleton while the overall quantity of β-$Mg_{17}Al_{12}$ was suppressed.
- The individual addition of Ca, Sr, and Ce to the AZ91 alloy as well as the combined inclusion of Ca and Sr to the alloy, the average grain size was lowered. Among all the squeezed cast AZ91-Ca-Sr, AZ91-Ca, and AZ91-Sr alloys, the AZ91-1wt.%Ca-0.6wt.%Sr alloy had the least average grain size (AGS =54 μm).

- During the individual addition of Ca and Sr, as well as combined addition of Ca and Sr, the hardness value appears to increase. This is because of the Al_2Ca and Al_4Sr intermetallics formation and increase in grain boundary density in AZ91-Ca, AZ91-Sr and AZ91-Ca-Sr alloys.
- Small particles are formed by the breakdown of large β-phase precipitates during extrusion. In the extrusion direction, the smaller Al-Sr, Al-Ca precipitates reposition themselves to generate stringers (AZ91-1wt%Ca-0.6wt%Sr alloy).
- After addition of Ca and Sr to extruded AZ91 alloy, the average grain size reduced from 8.52 μm to 6.14 μm. The amount of recrystallized grains increases after Ca and Sr addition.
- Reduced grain size influenced the yield asymmetry of extruded alloy and yield asymmetry is reduced after alloy addition (Ca and Sr).
- With addition of Ca to AZ91 alloy, Al_2Ca formation suppressed the β - phase and coarser β -$Mg_{17}Al_{12}$ phase transformed into skeleton type structure of interdendritic network. Formation of bright needle like Al_4Sr intermetallics after the addition of 1wt.%Sr to AZ91 alloy. After Ce addition to AZ91 alloy, rod like structure and a few spherical shaped $Al_{11}Ce_3$ intermetallics are formed which suppressed the β – phase and discontinuous network is observed.
- Reduction in average grain size, SDAS and suppression of the β-phase and slight improvement in hardness are observed after the addition of Ca, Sr and Ce to AZ91 alloy. AZ91-1wt.%Sr has the smallest average grain size (AGS = 41.31 μm).
- In the sample plate, the microhardness values for AZ91-Ca, AZ91-Sr, and AZ91-Ce were computed for three separate zones. For each alloy, the edge region exhibits the highest hardness value. The hardness of AZ91 increased with Ca, Sr and Ce additions. This occurred due to increase in grain boundary density as well as Al_2Ca, Al_4Sr and $Al_{11}Ce_3$ intermetallic formation in AZ91-1 wt.%

Ca, AZ91-1wt.%Sr and AZ91- 1wt.% Ce alloys, respectively. Considering centre region of the rod, the highest improvement of 10.83 % in hardness was obtained with Ce addition to AZ91 alloy.

6.2 Scope of future work

- Investigation can be done on squeeze cast alloys keeping the weight percentage of Sr constant and varying the Ca weight percentage.
- Effect of different heat treatments on microstructure and mechanical properties of AZ91 alloy with Ca ,Sr and Ce addition can be studied.
- Rare earth element addition to AZ91 alloy other than Ce can be studied.
- It requires thorough study to identify the optimal extrusion parameters that will improve the mechanical properties of the extruded AZ91 alloy after alloy addition.

Chapter 7

Contributions to the original knowledge

Prior literature has paid little attention to the combined effect of the alkaline earth elements strontium and calcium on the microstructure refinement and mechanical properties of the squeeze-cast as well as extruded AZ91 alloy. In order to be employed in automobiles body applications, new compositions for as-cast and extruded AZ91 Mg alloys with better squeeze casting process, refined microstructure, mechanical properties, and texture weakening are being developed.

- Tensile properties of squeeze cast AZ91 alloy at room temperature is enhanced due to high melt pouring temperature (700°C) and optimized applied pressure (100 MPa) during squeeze casting process. In this work, squeeze cast AZ91 alloys resulted in reduction of porosity in the cast alloys and more refined microstructure compared to die-cast AZ91 alloy.
- Combined addition of Ca and Sr results in more refined microstructure and reduction in grain size, which was not observed in individual effect of Ca and Sr to AZ91 alloy.
- It was determined that adding Ca and Sr weakens the texture of extruded AZ91 alloys. Particle stimulated nucleation (PSN), which produces grains with random orientations, is the cause of the texture weakening. As a result of evaluating the mechanical characteristics of the extruded alloy AZ91-1Ca-0.6Sr, the yield symmetry was decreased.
- Vickers microhardness test for squeeze cast alloys AZ91 ,AZ91-Ca , AZ91-Sr, AZ91-Ce was investigated in different zones of the sample plate showing that the hardness in the edge zone is greater than the centre zone for all the above mentioned alloys with 1wt%.

REFERENCES

[1] L. Shengfa, K. Liugen, H. Hui, W. Zhongfan, The Role of Calcium in Microstructural Refinement of AZ91 Magnesium Alloy, Journal of Wuhan University of Technology - Mater. Sci. Ed. 21 (4) (2006) 45-47.

[2] R. Xiao, W. Liu, G. Wu, L. Zhang, B. Liu, W. Ding, Effect of Ca content and rheo-squeeze casting parameters on microstructure and mechanical properties of AZ91−1Ce−xCa alloys, Trans. Nonferrous Met. Soc. China 31(2021) 1572−1586.

[3] A. SrinIvasan, Influence of Si, Sb and Sr additions on the Microstructure, Mechanical properties and Corrosion behavior of AZ91 Magnesium Alloy(2008).

[4] K. Hirai, H. Somekawa, Y. Takigawa, K. Higashi, Effects of Ca and Sr addition on mechanical properties of a cast AZ91 magnesium alloy at room and elevated temperature, Mater. Sci. Eng. A 403 (2005) 276–280.

[5] E. Tolouie, R. Jamaati, Effect of β–$Mg_{17}Al_{12}$ phase on microstructure, texture and mechanical properties of AZ91 alloy processed by asymmetric hot rolling, Mater. Sci. Eng. A S0921-5093(18)31297-8.

[6] A. S. Marodkar, H. Patil, H. Borkar, Effect of Squeeze Casting and Combined Addition of Calcium and Strontium on Microstructure and Mechanical Properties of AZ91 Magnesium Alloy, Int. J. Met. (2023) 1-19.

[7] Y. Cubides, A. I. Karayan, M.W. Vaughan, I. Karaman, H. Castaneda, Enhanced mechanical properties and corrosion resistance of a fine-grained Mg-9Al-1Zn alloy: the role of bimodal grain structure and β-Mg17Al12 precipitates, Materialia 13 (2020) 100840.

[8] Redeemina Comfort Bonnah, Yu Fu, Hai Hao, Microstructure and mechanical properties of AZ91 magnesium alloy with minor additions of Sm, Si and Ca elements .China Foundry 16, 319–325 (2019).

[9] Y. Zhang, G. Wu, W. Liu, L. Zhang, S. Pang, Y. Wang, W. Ding, Effects of processing parameters and Ca content on microstructure and mechanical properties of squeeze casting AZ91–Ca alloys, Mater. Sci. Eng. A 595 (2014) 109–117.

[10] W. Huang, H. Yan, Effect of Cerium Addition on Microstructure and Mechanical Properties of Die-cast AM60 Alloy, International Conference on Electronic & Mechanical Engineering and Information Technology (2011).

[11] Z. Feng, E. Wang, M. Zhang, X. Li and C. Su, Effect of Ce on Microstructure and Mechanical Properties of AZ91 Magnesium Alloy, JPCS 2174 (2022) 012060.

[12] C. Huisheng, G. Feng, R. Xiushan, S. Juan, C. Baodong, Effects of cerium on as-cast microstructure of AZ91 magnesium alloy under different solidification rates, J. Rare Earths, 34 (7) (2016) 736-741.

[13] Manufacturing processes for light alloys, G.T. Kridli1 , P.A. Friedman2 and J.M. Boileau

[14] Physical metallurgy of magnesium A. A. KAYA , Mugla University, Turkey

[15] Light alloys (5th edition), Ian Polmear , David St John, Jian-Feng Nie, Ma Qian(2017).

[16] https://blog.keronite.com/magnesium-alloys-uses-applications-and-benefits

[17] Qudong, W., Wenzhou, C., Xiaoqin, Z., Yizhen, L., Wenjiang, D., Yanping, Z., ... & Mabuchi, M. (2001). Effects of Ca addition on the microstructure and mechanical properties of AZ91magnesium alloy. Journal of materials science, 36, 3035-3040.

[18] Yu Fan, Guohua Wu, Hongtao Gao, Guanqun Li and Chunquan Zhai: J Mater. Sci., 2006 vol. 41, pp. 540

[19] Jereza, K., Brindle, R., Robison, S., Hryn, J. N., & Weiss, D. J. (1991). Bruce M. Cox: Proc. Magnesium Technology 2006, AA Luo. Mater. Sci. Eng, 134, 1197.

[20] S Lee, S H Lee and D H Kim: Metall. Mater. Trans. A, 1998, vol. 29A, pp.122.

[21] L. Shang et al., Effect of microalloying (Ca, Sr, and Ce) on elevated temperature tensile behavior of AZ31 magnesium sheet alloy , Materials Science & Engineering A (2011).

[22] Aria Afsharnaderi et al., Enhanced mechanical properties of as-cast AZ91 magnesium alloy by combined RE-Sr addition and hot extrusion, Materials Science & Engineering A (2020).

[23] Alireza Sadeghi , Majid Hoseini, Mihriban Pekguleryuz, Effect of Sr addition on texture evolution of Mg–3Al–1Zn (AZ31) alloy during extrusion , Materials Science and Engineering A 528 (2011) 3096–3104.

[24] H. Borkar et al., Effect of strontium on the texture and mechanical properties of extruded Mg–1%Mn alloys ,Materials Science and Engineering A, 549 (2012) 168– 175.

[25] A.E. Davis et al.,Reducing yield asymmetry and anisotropy in wrought magnesium alloys – A comparative study, Materials Science & Engineering A (2019).

[26] “The effect of strontium in plasticity of magnesium alloys”, K. Hazeli, A.Sadeghi, M.O.Pekguleryuz, A.Kontsos, Materials Science & Engineering A 578 (2013) 383–393

[27] Sadeghi, A., Hoseini, M., & Pekguleryuz, M. (2011). Effect of Sr addition on texture evolution of Mg–3Al–1Zn (AZ31) alloy during extrusion. Materials Science and Engineering: A, 528(7-8), 3096-3104.

[28] Sadeghi, A., & Pekguleryuz, M. (2011). Microstructure, mechanical properties and texture evolution of AZ31 alloy containing trace levels of strontium. Materials characterization, 62(8), 742-750.

[29] F.J. Humphreys, M. Hatherly, Recrystallization and Related Annealing Phenomena, Pergamon, Oxford, UK, 2004.

[30], Chaojie Chea, Zhongyi Caia, Xiaohong Yangb, Liren Cheng, Yunqiu Du, The effect of co-addition of Si, Ca and RE on microstructure and tensile properties of as-extruded AZ91 alloy

[31] Wenxian Huang, Hong Yan, Effect of Cerium Addition on Microstructure and Mechanical Properties of Die-cast AM60 Alloy.

[32] Cai Huisheng , Guo Feng , Ren Xiushan , Su Juan , Chen Baodong , Effects of cerium on as-cast microstructure of AZ91 magnesium alloy under different solidification rates.

[33] L. Shang, S. Yue, R. Verma, P. Krajewski, C. Galvani, E. Essadiqi, Effect of microalloying (Ca, Sr, and Ce) on elevated temperature tensile behavior of AZ31 magnesium sheet alloy, Mater. Sci. Eng. A 528 (10-11), 3761-3770 (2011).